SunQM-6s4: In {N,n} QM Field Theory, A Point Charge's Electric Field Can Be Represented by Either the Schrodinger Equation/Solution, Or A 3D Spherical Wave Packet, In Form of Born Probability

Yi Cao

e-mail: yicaojob@yahoo.com. ORCID: 0000-0002-4425-039X

Abstract

In the newly designed {N,n} QM field theory, the four fundamental forces were re-classified to be three pair of forces: E/RFe-force, G/RFg-force, S/RFs-force, and each pair of this force was hypothesized that can be represented by the Schrodinger equation/solution. In the current paper, I worked out that not only a point charge's static electric field electric field strength E ∝ 1/r^2, but also its potential field U ∝ 1/r, can be reconstituted by using the H-atom's Schrodinger equation/solution (in form of the radial Born probability density functions). A global fitting method was developed for this kind of curve fitting. In the reconstitution, the (normalized) radial Born probability density functions can be treated as the "unit vector base functions" of a high-dimensional Hilbert space (that covers from r → 0 to r = ∞). This result confirmed that, not only the point-centered mass (density) field (see SunQM-3 series), but also the point-centered force field (or potential field), can be directly described by Schrodinger equation/solution. The physical meaning of this result can be viewed in either the wave mechanics, or in the particle mechanics. This work also showed that all point-centered fields (including both the mass field and the force field) can be represented in the form of 3D spherical wave packet. Therefore, these two methods are equivalent. These results, plus the three pairs of force (E/RFe-force, G/RFg-force, S/RFs-force) description (see SunQM-6), the non-Born probability description (see SunQM-4 series) that equals to the re-explanation of the Born probability density as the collection of all elliptical orbital tracks (see SunQM-6s2), the 3D wave packet description and the dis-entanglement of the outmost shell (or the "general decaying" process, see SunQM-6s1, -6s2, -6s3, etc.), the "|nL0> elliptical/parabolic/hyperbolic orbital transition model" (see SunQM-6s2, -6s3), and the trick that using the high-frequency n' to pin-point any small region in the {N,n} QM field (see SunQM-3s11, -6s1, etc.), all together they formed the foundation of the newly designed {N,n} QM field theory.

Key Words: Quantum mechanics, {N,n} QM field theory, Schrodinger equation/solution, electric field, potential field

Introduction

The {N,n} QM studies have revealed that not only the formation of Solar system [1] ~ [16], but also the formation of the whole universe [17] ~ [25], can be explained by the {N,n} QM. The success of the {N,n} QM study made me to believe that "all mass entities (from the whole universe to a single quark) can be described by Schrodinger equation and solution" (see paper SunQM-3s11 section IX). Then I extend this idea to the force field, re-classified the four fundamental forces into three pairs: G/RFg-force, E/RFe-force and S/RFs-force, and proposed a new {N,n} QM field theory (i.e., all force fields can also be described by Schrodinger equation and solution [23]). In paper SunQM-6s2 [26], I tried to use the newly designed "|nL0>

elliptical orbital transition model" to describe a photon's emission and propagation process. In paper SunQM-6s3 [27], I extended that model to be the "|nL0> elliptical/parabolic/hyperbolic orbital transition model", and used it to describe many general "decay" processes in the macro-world as well as in the micro-world. In the current paper, I successfully reconstituted a single point charge's static electric field $|\vec{\mathbf{E}}| \propto 1/r^2$ and the potential field U ∝ 1/r by using Schrodinger equation/solution (in form of Born probability). Thus, it fully set down the foundation of the {N,n} QM field theory.

Note: QM means Quantum Mechanics. For {N,n} QM nomenclature as well as the general notes, please see SunQM-1 sections VII & VIII. Note: Microsoft Excel's number format is often used in this paper, for example: x^2 = x^2, 3.4E+12 = $3.4*10^{12}$ = 3.4×10^{12}, 5.6E-9 = $5.6*10^{-9}$. Note: The reading sequence for the (28 posted) SunQM series papers is: SunQM-1, 1s1, 1s2, 1s3, 2, 3, 3s1, 3s2, 3s6, 3s7, 3s8, 3s3, 3s9, 3s4, 3s10, 3s11, 4, 4s1, 4s2, 5, 5s1, 5s2, 7, 6, 6s1, 6s2, 6s3, and 6s4. Note: for all SunQM series papers, reader should check "SunQM-9s1: Updates and Q/A for SunQM series papers" for the most recent updates and corrections. Note: |n*l*m> means |n,*l*,m> QM state, "nLL" or |nLL> means |n,*l*,m> QM state with *l* = n-1 = L, and *m* = n-1 = L. "nL0" or |nL0> means |n,*l*,m> QM state with *l* = n-1 = L, and m = 0. Note: RF means "RotaFusion", or "rotation diffusion". Note: NBP means non-Born probability. Note: Unless specified, the Schrodinger equation/solution (or the Born probability density radial function) mentioned in this paper (and in almost all of SunQM series papers) comes from the H-atom's electric potential, or at least using the potential function of U ∝ 1/r in the Schrodinger equation.

I. Using H-atom's radial Born probability with several super shells of {N,n=1..5//6}o QM structure to reconstitute a point charge's static electric field by fitting to E ∝ 1/r^2 curve

In the paper SunQM-6, I re-classified the four fundamental forces (Gravity, Electromagnetic, Strong, Weak, abbreviated as G-, E/M-, S-, W-force) to be three pair of forces: E/RFe-force, G/RFg-force, S/RFs-force. Then I hypothesized that each of these E/RFe-force, G/RFg-force, and S/RFs-force pairs should can be described by the Schrodinger equation/solution, i.e., the |n,*l*,m> QM state, in the form of either the Born probability 3D density, or the non-Born probability (NBP) 3D density. This forms the foundation of the newly designed {N,n} QM field theory.

In SunQM-6's Table-2 and eq-1, I had (conceptually) used the combination of multiple n(s) of |n,*l*,m> QM states to describe the QM mode of the E-force (i.e., the electric field $\vec{\mathbf{E}}$ vector) and the RFe-force (i.e., the magnetic field $\vec{\mathbf{B}}$ vector). In SunQM-6's Fig-9a, I used SunQM-6's eq-1 with $a_{nlm} \equiv 1$, (i.e., $\Sigma[r^2 |R(n,l)|^2]$), to reconstitute (or to fit) a single point charge's either $|\vec{\mathbf{E}}| \propto 1/r^2$ or U ∝ 1/r curve, and it was failed (due to the $a_{nlm} \equiv 1$. Note: it equivalents to $b_{nlm} = b_n \equiv 1$ in eq-1). In the current paper, I improved fitting by allowing $b_{nlm} = b_n$ to be free (or, by manually adjusting the possible values during fitting, see the column 23 and row 2 ~ 6 in Table 1), and also adapted the {N,n=1..5//6}o QM structure so that each N super shell contains only five n shells (n =1, 2, 3, 4, 5), and thus built the eq-1:

$$\sum_{N\to-\infty}^{N\to\infty} a_N \left[\sum_{n=1}^{n=5} b_n |n,l,m\rangle\right] \qquad \text{eq-1}$$

or, quantitatively (using the Born probability radial function), as shown in eq-2

$$\sum_{N\to-\infty}^{N\to\infty} a_N \left[\sum_{n=1}^{n=5} b_n r_N{}^2 |R(n,l)|^2\right] \qquad \text{eq-2}$$

where the b_n is the coefficient for each n state's $r_N{}^2|R(n,l)|^2$; a_N is the coefficient for each N super shell's $\sum_{n=1}^{n=5} b_n r_N{}^2|R(n,l)|^2$; and the definition of r_N is: while calculating the $r^2|R(n,l)|^2$, r_N = r; while plotting the eq-2 against the whole r range (0 < r < ∞), for each N super shell, $r_N = r * 36^N$ (see eq-4 and Table 2 for example). Figure 1a showed the radial Born probability function curves of $r^2|R(n,l)|^2$ from n = 1 to 5. (Note: $r^2|R(n,l)|^2$ has a physical unit of (1/r). After integration over dr, it has a zero physical unit). (Note: For the source of radial wave functions $R(n,l)$ from n = 1 to 5, see SunQM-3's section I-e).

I-a. Manually fit eq-2 to $|\vec{\mathbf{E}}| \propto 1/r^2$

In Table 1 (columns 1~ 24), I first used only one super shell of {N,n=1..5//6}o QM structure (supposing N=0 and r_1 = 1, so it is {0,n=1..5//6}o super shell) to fit to (or, to reconstitute) the electric field strength $|\vec{\mathbf{E}}| \propto 1/r^2$ curve. After manually adjusted to b_1= 95, b_2 = 7, b_3= 1.3, b_4= 0.5, b_5= 0.2, and divided whole curve by 95 (or $a_{N=0}$ = 1/95), (see the column 23 and row 2 ~ 7 in Table 1), the whole Born probability radial function becomes eq-3

$$\sum_{n=1}^{n=5} b_n\, r^2|R(n,l)|^2 = \frac{1}{95}[95r^2|R(1,0)|^2 + 7r^2|R(2,l)|^2 + 1.3r^2|R(3,l)|^2 + 0.5r^2|R(4,l)|^2 + 0.2r^2|R(5,l)|^2]$$

eq-3

(where l = 0..n-1. For example, $9r^2|R(2,l)|^2 = 9r^2|R(2,0)|^2 + 9r^2|R(2,1)|^2$). The obtained curve (see the red solid-line curve in Figure 1b, data from the column 23 in Table 1) fits to the $|\vec{\mathbf{E}}| \propto 1/r^2$ curve (see the black dotted-line curve in Figure 1b, data from the column 22 in Table 1) quite well in the range of $3 \le r \le 50$. (Note: Due to the amplitude of eq-3 is in an arbitrary scale, a single point charge's static $|\vec{\mathbf{E}}| = \frac{1}{4\pi\varepsilon_0}\frac{Q}{r^2}$ can be simplified to be a $\frac{1}{r^2}$ curve during the fitting). (Note: In {N,n} QM, "all mass between r_n and r_{n+1} belongs to orbit n" (see SunQM-3s2), so at r_1 = 1, a {0,n=1..5//6}o QM structure may can be said that it effectively starts from r = r_1 = 1 and ends at $r = r_1n^2 = r_16^2 = 36r_1$= 36. Therefore, the above "good fitting in range of $3 \le r \le 50$" by using a single {N,n//6} super shell (with r_1 = 1) will be more formalized if it is said as a "good fitting in range of $1 \le r \le 36$").

When re-plotting Figure 1b with the log(r), (see the red dashed line curve vs. black dotted line curve in Figure 1c), it clearly showed that under r < 1, the fitting was completely off. To compensate for that, we added a second super shell of {-1,n=1..5//6}o QM structure into eq-3 (on top of the first super shell of {0,n=1..5//6}o QM structure) for the fitting (see Table 2). Because N = 0 super shell covered the fitting range of $1 \le r \le 36$, the new N= -1 super shell should be able to cover the fitting range of $\frac{1}{36} \le r \le 1$. In Table 2, after manually adjusted to b_1= 110, b_2 = 12, b_3= 2, b_4= 0.7, b_5= 0.1, and divided whole curve by 0.1 (or $a_{N=-1}$ = 1/0.1, see the column 24 and row 2 ~ 7 in Table 2), the whole Born probability radial function becomes

$$\sum_{N=-1}^{N=0} a_N \left[\sum_{n=1}^{n=5} b_n\, {r_N}^2|R(n,l)|^2\right] =$$

$$\frac{1}{0.1}[101{r_{N=-1}}^2|R(1,0)|^2 + 12{r_{N=-1}}^2|R(2,l)|^2 + 2{r_{N=-1}}^2|R(3,l)|^2 + 0.7{r_{N=-1}}^2|R(4,l)|^2 + 0.1{r_{N=-1}}^2|R(5,l)|^2] +$$
$$\frac{1}{95}[95r^2|R(1,0)|^2 + 7r^2|R(2,l)|^2 + 1.3r^2|R(3,l)|^2 + 0.5r^2|R(4,l)|^2 + 0.2r^2|R(5,l)|^2]$$

eq-4

Notice that the meaning of $r_{N=-1}$ in eq-4 is: when doing the ${r_{N=-1}}^2|R(n,l)|^2$ calculation, $r_{N=-1}$ = r (see column 2 in Table 2); when plotting the curve of eq-4, $r_{N=-1} = r * 36^N = \frac{r}{36}$ for the N = -1 super shell (see column 1 in Table 2). Figure 1c (the red solid line curve) showed that eq-4 fitted to the $|\vec{\mathbf{E}}| \propto 1/r^2$ curve quite well in the range of $\frac{1}{36} \le r \le 36$. However, when extended r down to $\frac{1}{36^2}$, the fitting curve was completely off again from the $1/r^2$ curve (see the red solid line curve in Figure 1d). Then, I added the 3rd N super shell {-2,n//6} to cover the r range of $\frac{1}{36^2} \le r \le \frac{1}{36}$. After manually adjusted to b_1= 200, b_2 = 12, b_3= 2, b_4= 0.7, b_5= 0.1, and $a_{N=-2}$ = 1/0.000085 (the data table was not shown here), it fitted the $|\vec{\mathbf{E}}| \propto 1/r^2$ curve quite well within the range of $\frac{1}{36^2} \le r \le 36$ (see the green solid line curve in Figure 1d). So now, we can understand that, by adding more and more N super shells with N = -3, -4, …, down to -∞, we can push the good fitting range down to $r \to 0$. Similarly, by

adding more and more N super shells with N = +1, +2, …, up to +∞, we can push the good fitting range up to r → ∞. This is exactly the eq-2 expressed. Thus, we have (roughly) proved that with the eq-2, we are able to use the Schrodinger equation/solution's redial wave function, (i.e., the Born probability's r-1D density function) to reconstitute (or to fit, or to represent) $|\vec{\mathbf{E}}| \propto 1/r^2$ for the range of 0 < r < +∞.

Table 1. Use eq-2 with a single N super shell {0,n=1..5//6}o QM to fit to $|\vec{\mathbf{E}}| \propto 1/r^2$ curve.

																			rn			fit to 1/r^2			fit to 1/r	
																			1		b_1 =	95		b_1 =	40	
																			4		b_2 =	7		b_2 =	15	
																			9		b_3 =	1.3		b_3 =	7	
																			16		b_4 =	0.5		b_4 =	4	
For the 1st super shell, N = 0																			25		b_5 =	0.2		b_5 =	2	
																					devided	95		devided	32	
r_1=	1.000																			1	1					
r =	r^2*|R(1,0)|^2	r^2*|R(2,0)|^2	r^2*|R(2,1)|^2	r^2*|R(3,0)|^2	r^2*|R(3,1)|^2	r^2*|R(3,2)|^2	r^2*|R(4,0)|^2	r^2*|R(4,1)|^2	r^2*|R(4,2)|^2	r^2*|R(4,3)|^2	r^2*|R(5,0)|^2	r^2*|R(5,1)|^2	r^2*|R(5,2)|^2	r^2*|R(5,3)|^2	r^2*|R(5,4)|^2	Σ(n=1..2)	Σ(n=1..3)	Σ(n=1..4)	Σ(n=1..5)	U ∝ 1/r	E ∝ 1/r^2	{N=0,n//6}, fit E	ΔΣ, {0,n//6}, fit E		{N=0,n//6}, fit U	ΔΣ, {{0,n//6}, fit U
0.01	3.92E-04	4.90E-05	4.13E-10	1.45E-05	1.45E-10	8.07E-17	6.13E-06	6.45E-11	4.85E-17	4.82E-24	3.14E-06	3.38E-11	2.85E-17	4.14E-24	1.15E-31	4.41E-04	4.56E-04	4.62E-04	4.65E-04	1.00E+02	1.00E+04	3.96E-04	1.00E+04		5.17E-04	1.00E+02
0.02	1.54E-03	1.92E-04	6.53E-09	5.69E-05	2.29E-09	5.13E-15	2.40E-05	1.02E-09	3.08E-15	1.23E-21	1.23E-05	5.35E-10	1.81E-15	1.05E-21	1.17E-28	1.73E-03	1.79E-03	1.81E-03	1.82E-03	5.00E+01	2.50E+03	1.55E-03	2.50E+03		2.03E-03	5.00E+01
0.03	3.39E-03	4.24E-04	3.28E-08	1.26E-04	1.15E-08	5.81E-14	5.30E-05	5.12E-09	3.49E-14	3.13E-20	2.71E-05	2.68E-09	2.05E-14	2.69E-20	6.74E-27	3.81E-03	3.94E-03	3.99E-03	4.02E-03	3.33E+01	1.11E+03	3.42E-03	1.11E+03		4.47E-03	3.33E+01
0.04	5.91E-03	7.38E-04	1.02E-07	2.19E-04	3.60E-08	3.24E-13	9.23E-05	1.60E-08	1.95E-13	3.11E-19	4.72E-05	8.39E-09	1.14E-13	2.67E-19	1.19E-25	6.65E-03	6.86E-03	6.96E-03	7.00E-03	2.50E+01	6.25E+02	5.97E-03	6.25E+02		7.79E-03	2.50E+01
0.06	1.28E-02	1.59E-03	5.09E-07	4.73E-04	1.79E-07	3.64E-12	1.99E-04	7.95E-08	2.19E-12	7.90E-18	1.02E-04	4.17E-08	1.29E-12	6.78E-18	6.82E-24	1.44E-02	1.48E-02	1.50E-02	1.51E-02	1.67E+01	2.78E+02	1.29E-02	2.78E+02		1.68E-02	1.66E+01
0.08	2.18E-02	2.72E-03	1.58E-06	8.06E-04	5.53E-07	2.02E-11	3.40E-04	2.46E-07	1.21E-11	7.81E-17	1.74E-04	1.29E-07	7.13E-12	6.71E-17	1.20E-22	2.45E-02	2.53E-02	2.57E-02	2.59E-02	1.25E+01	1.56E+02	2.20E-02	1.56E+02		2.88E-02	1.25E+01
0.1	3.27E-02	4.08E-03	3.77E-06	1.21E-03	1.32E-06	7.60E-11	5.10E-04	5.89E-07	4.57E-11	4.61E-16	2.61E-04	3.09E-07	2.68E-11	3.96E-16	1.11E-21	3.68E-02	3.80E-02	3.86E-02	3.88E-02	1.00E+01	1.00E+02	3.31E-02	1.00E+02		4.32E-02	9.96E+00
0.2	1.07E-01	1.33E-02	5.46E-05	3.92E-03	1.91E-05	4.55E-09	1.65E-03	8.52E-06	2.73E-09	1.12E-13	8.46E-04	4.46E-06	1.61E-09	9.64E-14	1.09E-18	1.21E-01	1.25E-01	1.26E-01	1.27E-01	5.00E+00	2.50E+01	1.08E-01	2.49E+01		1.41E-01	4.86E+00
0.3	1.98E-01	2.41E-02	2.50E-04	7.10E-03	8.76E-05	4.85E-08	2.99E-03	3.89E-05	2.91E-08	2.74E-12	1.53E-03	2.04E-05	1.71E-08	2.35E-12	6.05E-17	2.22E-01	2.29E-01	2.32E-01	2.34E-01	3.33E+00	1.11E+01	1.99E-01	1.09E+01		2.60E-01	3.07E+00
0.4	2.88E-01	3.43E-02	7.15E-04	1.01E-02	2.50E-04	2.55E-07	4.24E-03	1.11E-04	1.53E-07	2.60E-11	2.17E-03	5.82E-05	8.98E-08	2.23E-11	1.03E-15	3.23E-01	3.33E-01	3.37E-01	3.40E-01	2.50E+00	6.25E+00	2.90E-01	5.96E+00		3.79E-01	2.12E+00
0.5	3.68E-01	4.26E-02	1.58E-03	1.25E-02	5.51E-04	9.10E-07	5.23E-03	2.44E-04	5.46E-07	1.47E-10	2.67E-03	1.28E-04	3.20E-07	1.27E-10	9.24E-15	4.12E-01	4.25E-01	4.31E-01	4.33E-01	2.00E+00	4.00E+00	3.71E-01	3.63E+00		4.84E-01	1.52E+00
0.7	4.83E-01	5.14E-02	4.97E-03	1.48E-02	1.72E-03	6.00E-06	6.16E-03	7.61E-04	3.59E-06	1.97E-09	3.14E-03	3.98E-04	2.10E-06	1.69E-09	2.47E-13	5.40E-01	5.56E-01	5.63E-01	5.67E-01	1.43E+00	2.04E+00	4.88E-01	1.55E+00		6.35E-01	7.93E-01
1	5.41E-01	4.60E-02	1.53E-02	1.26E-02	5.22E-03	4.17E-05	5.18E-03	2.30E-03	2.49E-05	2.94E-08	2.62E-03	1.20E-03	1.46E-05	2.52E-08	7.75E-12	6.03E-01	6.21E-01	6.28E-01	6.32E-01	1.00E+00	1.00E+00	5.46E-01	4.54E-01		7.11E-01	2.89E-01
1.4	4.77E-01	2.17E-02	3.95E-02	5.12E-03	1.30E-02	2.41E-04	1.99E-03	5.65E-03	1.42E-04	3.55E-07	9.77E-04	2.93E-03	8.31E-05	3.03E-07	1.91E-10	5.38E-01	5.56E-01	5.64E-01	5.68E-01	7.14E-01	5.10E-01	4.82E-01	2.86E-02		6.30E-01	8.44E-02
1.8	3.54E-01	2.68E-03	7.23E-02	2.31E-04	2.27E-02	8.33E-04	4.99E-05	9.69E-03	4.88E-04	2.17E-06	1.71E-05	4.99E-03	2.83E-04	1.85E-06	2.01E-09	4.29E-01	4.53E-01	4.63E-01	4.68E-01	5.56E-01	3.09E-01	3.60E-01	-5.14E-02		4.85E-01	7.10E-02
2.2	2.38E-01	2.68E-03	1.08E-01	1.93E-03	3.17E-02	2.13E-03	1.02E-03	1.32E-02	1.23E-03	8.85E-06	5.70E-04	6.73E-03	7.09E-04	7.50E-06	1.27E-08	3.49E-01	3.84E-01	4.00E-01	4.08E-01	4.55E-01	2.07E-01	2.46E-01	-3.98E-02		3.59E-01	9.52E-02
2.6	1.49E-01	2.26E-02	1.41E-01	9.57E-03	3.79E-02	4.44E-03	4.45E-03	1.53E-02	2.52E-03	2.76E-05	2.37E-03	7.66E-03	1.44E-03	2.32E-05	5.77E-08	3.13E-01	3.65E-01	3.87E-01	3.99E-01	3.85E-01	1.48E-01	1.62E-01	-1.42E-02		2.78E-01	1.06E-01
3	8.92E-02	5.60E-02	1.68E-01	2.00E-02	4.01E-02	8.02E-03	8.86E-03	1.55E-02	4.47E-03	7.09E-05	4.62E-03	7.57E-03	2.53E-03	5.94E-05	2.06E-07	3.13E-01	3.81E-01	4.10E-01	4.25E-01	3.33E-01	1.11E-01	1.07E-01	4.25E-03		2.36E-01	9.73E-02
3.6	3.87E-02	1.13E-01	1.91E-01	3.37E-02	3.57E-02	1.61E-02	1.40E-02	1.24E-02	8.61E-03	2.26E-04	7.07E-03	5.77E-03	4.79E-03	1.87E-04	1.00E-06	3.43E-01	4.29E-01	4.64E-01	4.82E-01	2.78E-01	7.72E-02	6.25E-02	1.46E-02		2.15E-01	6.24E-02
4	2.15E-02	1.47E-01	1.95E-01	3.82E-02	2.89E-02	2.31E-02	1.50E-02	9.02E-03	1.20E-02	4.30E-04	7.43E-03	3.96E-03	6.60E-03	3.52E-04	2.45E-06	3.63E-01	4.54E-01	4.90E-01	5.08E-01	2.50E-01	6.25E-02	4.81E-02	1.44E-02		2.13E-01	3.75E-02
4.5	1.00E-02	1.76E-01	1.90E-01	3.73E-02	1.87E-02	3.36E-02	1.35E-02	4.62E-03	1.67E-02	8.59E-04	6.40E-03	1.77E-03	8.96E-03	6.95E-04	6.51E-06	3.76E-01	4.65E-01	5.01E-01	5.19E-01	2.22E-01	4.94E-02	3.84E-02	1.10E-02		2.09E-01	1.32E-02
5	4.54E-03	1.90E-01	1.75E-01	3.06E-02	9.06E-03	4.53E-02	9.77E-03	1.30E-03	2.13E-02	1.55E-03	4.33E-03	3.21E-04	1.11E-02	1.24E-03	1.53E-05	3.70E-01	4.55E-01	4.88E-01	5.05E-01	2.00E-01	4.00E-02	3.28E-02	7.19E-03		2.01E-01	-6.58E-04
6	8.85E-04	1.78E-01	1.34E-01	1.09E-02	0.00E+00	6.95E-02	1.75E-03	1.05E-03	2.84E-02	4.05E-03	4.76E-04	1.05E-03	1.38E-02	3.11E-03	6.34E-05	3.13E-01	3.94E-01	4.29E-01	4.47E-01	1.67E-01	2.78E-02	2.52E-02	2.56E-03		1.71E-01	-3.97E-03
7.2	1.16E-04	1.31E-01	8.36E-02	1.01E-04	1.29E-02	9.32E-02	1.64E-03	1.10E-02	2.97E-02	9.56E-03	1.49E-03	6.80E-03	1.26E-02	6.91E-03	2.43E-04	2.15E-01	3.21E-01	3.73E-01	4.01E-01	1.39E-01	1.93E-02	1.77E-02	1.59E-03		1.32E-01	6.74E-03
8	2.88E-05	9.66E-02	5.73E-02	7.60E-03	3.22E-02	1.03E-01	8.14E-03	1.95E-02	2.60E-02	1.49E-02	5.32E-03	1.07E-02	9.61E-03	1.02E-02	5.06E-04	1.54E-01	2.97E-01	3.65E-01	4.02E-01	1.25E-01	1.56E-02	1.38E-02	1.87E-03		1.14E-01	1.08E-02
9	4.93E-06	6.12E-02	3.37E-02	2.97E-02	5.95E-02	1.07E-01	1.88E-02	2.68E-02	1.80E-02	2.32E-02	1.04E-02	1.28E-02	4.91E-03	1.48E-02	1.10E-03	9.50E-02	2.91E-01	3.78E-01	4.22E-01	1.11E-01	1.23E-02	1.02E-02	2.11E-03		1.01E-01	1.00E-02
10.8	1.94E-07	2.30E-02	1.16E-02	7.68E-02	9.51E-02	9.63E-02	2.78E-02	2.34E-02	3.50E-03	4.05E-02	1.18E-02	7.81E-03	1.14E-05	2.17E-02	3.32E-03	3.46E-02	3.03E-01	3.98E-01	4.43E-01	9.26E-02	8.57E-03	6.82E-03	1.76E-03		8.96E-02	3.01E-03
12	2.17E-08	1.11E-02	5.31E-03	9.62E-02	1.02E-01	8.14E-02	2.23E-02	1.34E-02	0.00E+00	5.16E-02	7.07E-03	2.51E-03	1.86E-03	2.36E-02	5.89E-03	1.64E-02	2.96E-01	3.83E-01	4.24E-01	8.33E-02	6.94E-03	5.58E-03	1.37E-03		8.23E-02	1.07E-03
14.4	2.58E-10	2.22E-03	9.99E-04	9.51E-02	8.35E-02	4.91E-02	3.12E-03	1.34E-05	1.30E-02	6.69E-02	8.32E-06	1.90E-03	1.36E-02	1.90E-02	1.40E-02	3.22E-03	2.31E-01	3.14E-01	3.62E-01	6.94E-02	4.82E-03	3.89E-03	9.31E-04		6.47E-02	4.72E-03
16	1.30E-11	7.06E-04	3.07E-04	7.64E-02	6.21E-02	3.18E-02	5.96E-04	5.73E-03	3.05E-02	6.98E-02	4.11E-03	9.45E-03	2.00E-02	1.19E-02	2.11E-02	1.01E-03	1.71E-01	2.78E-01	3.44E-01	6.25E-02	3.91E-03	3.11E-03	8.00E-04		5.52E-02	7.29E-03
18	3.01E-13	1.58E-04	6.66E-05	4.98E-02	3.78E-02	1.70E-02	1.41E-02	2.55E-02	5.12E-02	6.59E-02	1.46E-02	1.89E-02	2.00E-02	3.42E-03	3.08E-02	2.25E-04	1.05E-01	2.62E-01	3.49E-01	5.56E-02	3.09E-03	2.46E-03	6.29E-04		4.81E-02	7.50E-03
20	6.80E-15	3.34E-05	1.37E-05	2.87E-02	2.06E-02	8.43E-03	3.64E-02	4.73E-02	6.31E-02	5.63E-02	2.08E-02	2.04E-02	1.26E-02	0.00E+00	3.97E-02	4.71E-05	5.78E-02	2.61E-01	3.54E-01	5.00E-02	2.50E-03	2.06E-03	4.40E-04		4.39E-02	6.11E-03
25.2	3.28E-19	4.86E-07	1.91E-07	4.64E-03	3.06E-03	1.05E-03	6.40E-02	6.16E-02	5.10E-02	2.66E-02	4.20E-03	1.23E-03	1.08E-03	1.92E-02	5.00E-02	6.77E-07	8.75E-03	2.12E-01	2.88E-01	3.97E-02	1.57E-03	1.35E-03	2.26E-04		3.20E-02	7.64E-03
28	1.50E-21	4.58E-08	1.77E-08	1.48E-03	9.45E-04	3.06E-04	5.38E-02	4.80E-02	3.48E-02	1.52E-02	3.51E-04	2.44E-03	1.21E-02	3.44E-02	4.68E-02	6.35E-08	2.73E-03	1.55E-01	2.51E-01	3.57E-02	1.28E-03	1.04E-03	2.37E-04		2.56E-02	1.01E-02
32	6.57E-25	1.46E-09	5.53E-10	2.54E-04	1.57E-04	4.74E-05	3.11E-02	2.58E-02	1.64E-02	5.99E-03	1.63E-02	2.22E-02	3.42E-02	4.55E-02	3.59E-02	2.01E-09	4.58E-04	7.97E-02	2.34E-01	3.13E-02	9.77E-04	7.48E-04	2.29E-04		1.96E-02	1.16E-02
36	2.79E-28	4.34E-11	1.62E-11	3.86E-05	2.32E-05	6.68E-06	1.41E-02	1.12E-02	6.48E-03	2.08E-03	3.74E-02	4.09E-02	4.50E-02	4.19E-02	2.36E-02	5.97E-11	6.85E-05	3.39E-02	2.23E-01	2.78E-02	7.72E-04	5.77E-04	1.95E-04		1.60E-02	1.17E-02
40	1.16E-31	1.23E-12	4.53E-13	5.36E-06	3.16E-06	8.73E-07	5.43E-03	4.16E-03	2.24E-03	6.54E-04	4.51E-02	4.46E-02	4.10E-02	3.07E-02	1.36E-02	1.68E-12	9.39E-06	1.25E-02	1.88E-01	2.50E-02	6.25E-04	4.34E-04	1.91E-04		1.25E-02	1.25E-02
50.4	1.70E-40	9.62E-17	3.48E-17	2.33E-08	1.32E-08	3.41E-09	2.69E-04	1.94E-04	9.32E-05	2.29E-05	2.04E-02	1.78E-02	1.29E-02	7.03E-03	2.15E-03	1.31E-16	3.99E-08	5.79E-04	6.09E-02	1.98E-02	3.94E-04	1.30E-04	2.64E-04		3.84E-03	1.60E-02

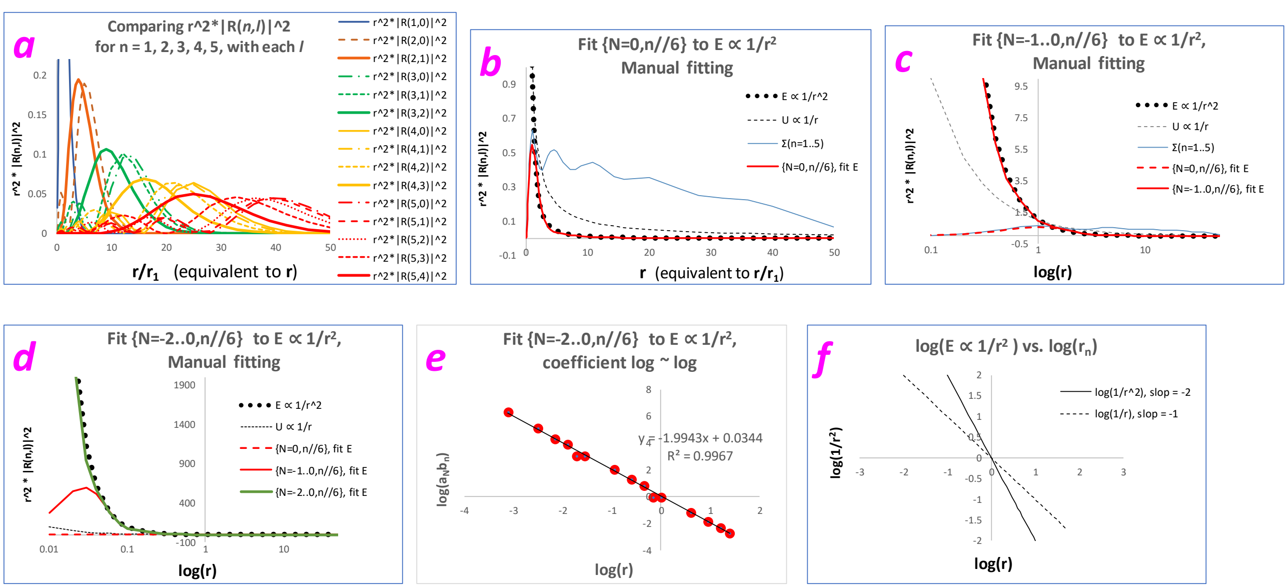

Figure 1a. Comparing radial Born probability density function $r^2|R(n,l)|^2$ for n = 1, 2, 3, 4, and 5 (with different *l* quantum numbers).

Figure 1b. (Manual fitting) Use eq-2 with a single N super shell {0,n=1..5//6}o QM to fit to $|\vec{\mathbf{E}}| \propto 1/r^2$ curve (see the red solid-line curve vs. the black dotted curve). For the blue solid-line, it was eq-2 with $a_N b_n \equiv 1$ (see SunQM-6's Fig-9a).

Figure 1c. (Manual fitting) Use eq-2 with two N super shells {N=-1..0,n=1..5//6}o QM to fit to $|\vec{\mathbf{E}}| \propto 1/r^2$ curve (see the red solid-line curve vs. the black dotted curve).

Figure 1d. (Manual fitting) Use eq-2 with three N super shells {N=-2..0,n=1..5//6}o QM to fit to $|\vec{\mathbf{E}}| \propto 1/r^2$ curve (see the green solid-line curve vs. the black dotted curve).

Figure 1e. (Manual fitting) A plot of log($a_N b_n$) vs. log(r) by using the eq-2's coefficient $a_N b_n$ in Figure 1d (see the red dots). The black solid line is the linear regression.

Figure 1f. A plot for log(1/r^2) vs. log(r), see the solid line; and for log(1/r) vs. log(r), see the dashed line.

Table 2. Use eq-2 with two N super shells {N=-1..0,n=1..5//6}o QM to fit to $|\vec{\mathbf{E}}| \propto 1/r^2$ curve.

rn		fit to 1/r^2
1	b_1 =	110
4	b_2 =	12
9	b_3 =	2
16	b_4 =	0.7
25	b_5 =	0.1
	devided	0.1

	fit to 1/r
b_1 =	40
b_2 =	14
b_3 =	6
b_4 =	2.5
b_5 =	1
devided	0.8

For 2nd super shell, N = -1 (plus N = 0 super shell)

	r_1=	1.000																					1	1			
r/36	r =	r^2*|R(1,0)|^2	r^2*|R(2,0)|^2	r^2*|R(2,1)|^2	r^2*|R(3,0)|^2	r^2*|R(3,1)|^2	r^2*|R(3,2)|^2	r^2*|R(4,0)|^2	r^2*|R(4,1)|^2	r^2*|R(4,2)|^2	r^2*|R(4,3)|^2	r^2*|R(4,0)|^2	r^2*|R(5,1)|^2	r^2*|R(5,2)|^2	r^2*|R(5,3)|^2	r^2*|R(5,4)|^2	Σ(n=1..2)	Σ(n=1..3)	Σ(n=1..4)	Σ(n=1..5)	U ∝ 1/r	E ∝ 1/r^2	{N=-1..0,n//6), fit E	Δ{, {-1,n)+{0,n), fit U	{N=-1..0,n//6), fit U	Δ{, {-1,n)+{0,n), fit U
0.01	0.36	2.52E-01	3.04E-02	4.88E-04	8.95E-03	1.71E-04	1.39E-07	3.76E-03	7.59E-05	8.35E-08	1.14E-11	1.93E-03	3.98E-05	4.90E-08	9.80E-12	3.66E-16	2.83E-01	2.92E-01	2.96E-01	2.98E-01	1.00E+02	1.00E+04	2.81E+02	9718.5	1.32E+01	86.8
0.02	0.72	4.91E-01	5.17E-02	5.45E-03	1.48E-02	1.88E-03	7.01E-06	6.18E-03	8.34E-04	4.19E-06	2.44E-09	3.15E-03	4.36E-04	2.46E-06	2.09E-09	3.24E-13	5.48E-01	5.65E-01	5.72E-01	5.76E-01	5.00E+01	2.50E+03	5.48E+02	1952.33	2.57E+01	24.3
0.03	1.08	5.38E-01	4.19E-02	1.93E-02	1.13E-02	6.52E-03	6.28E-05	4.61E-03	2.86E-03	3.74E-05	5.22E-08	2.32E-03	1.49E-03	2.19E-05	4.47E-08	1.62E-11	5.99E-01	6.17E-01	6.25E-01	6.28E-01	3.33E+01	1.11E+03	6.00E+02	511.49	2.81E+01	5.2
0.04	1.44	4.66E-01	1.93E-02	4.24E-02	4.41E-03	1.39E-02	2.78E-04	1.69E-03	6.04E-03	1.64E-04	4.36E-07	8.26E-04	3.13E-03	9.57E-05	3.72E-07	2.49E-10	5.27E-01	5.46E-01	5.54E-01	5.58E-01	2.50E+01	6.25E+02	5.20E+02	104.99	2.45E+01	0.5
0.06	2.16	2.48E-01	1.72E-03	1.05E-01	1.46E-03	3.09E-02	1.96E-03	7.89E-04	1.29E-02	1.13E-03	7.79E-06	4.48E-04	6.59E-03	6.54E-04	6.61E-06	1.08E-08	3.55E-01	3.89E-01	4.04E-01	4.11E-01	1.67E+01	2.78E+02	2.87E+02	-8.82	1.46E+01	2.1
0.08	2.88	1.05E-01	4.51E-02	1.61E-01	1.68E-02	3.99E-02	6.80E-03	7.53E-03	1.56E-02	3.81E-03	5.43E-05	3.95E-03	7.71E-03	2.17E-03	4.56E-05	1.43E-07	3.11E-01	3.74E-01	4.01E-01	4.15E-01	1.25E+01	1.56E+02	1.41E+02	15.04	9.44E+00	3.1
0.1	3.6	3.87E-02	1.13E-01	1.91E-01	3.37E-02	3.57E-02	1.61E-02	1.40E-02	1.24E-02	8.61E-03	2.26E-04	7.07E-03	5.77E-03	4.79E-03	1.87E-04	1.00E-06	3.43E-01	4.29E-01	4.64E-01	4.82E-01	1.00E+01	1.00E+02	8.11E+01	18.88	8.08E+00	1.92
0.2	7.2	1.16E-04	1.31E-01	8.36E-02	1.01E-04	1.29E-02	9.32E-02	1.64E-03	1.10E-02	2.97E-02	9.56E-03	1.49E-03	6.80E-03	1.26E-02	6.91E-03	2.43E-04	2.15E-01	3.21E-01	3.73E-01	4.01E-01	5.00E+00	2.50E+01	2.85E+01	-3.4820	4.89E+00	0.106
0.3	10.8	1.94E-07	2.30E-02	1.16E-02	7.68E-02	9.51E-02	9.63E-02	2.78E-02	2.34E-02	3.50E-03	4.05E-02	1.18E-02	7.81E-03	1.14E-05	2.17E-02	3.32E-03	3.46E-02	3.03E-01	3.98E-01	4.43E-01	3.33E+00	1.11E+01	1.04E+01	0.6840	3.23E+00	0.1024
0.4	14.4	2.58E-10	2.22E-03	9.99E-04	9.51E-02	8.35E-02	4.91E-02	3.12E-03	1.34E-05	1.30E-02	6.69E-02	8.32E-06	1.90E-03	1.36E-02	1.90E-02	1.40E-02	3.22E-03	2.31E-01	3.14E-01	3.62E-01	2.50E+00	6.25E+00	5.86E+00	0.3901	2.46E+00	0.0372
0.5	18	3.01E-13	1.58E-04	6.66E-05	4.98E-02	3.78E-02	1.70E-02	1.41E-02	2.55E-02	5.12E-02	6.59E-02	1.46E-02	1.89E-02	2.00E-02	3.42E-03	3.08E-02	2.25E-04	1.05E-01	2.62E-01	3.49E-01	2.00E+00	4.00E+00	3.67E+00	0.3253	1.87E+00	0.1281
0.7	25.2	3.28E-19	4.86E-07	1.91E-07	4.64E-03	3.06E-03	1.05E-03	6.40E-02	6.16E-02	5.10E-02	2.66E-02	4.20E-03	1.23E-03	1.08E-03	1.92E-02	5.00E-02	6.77E-07	8.75E-03	2.12E-01	2.88E-01	1.43E+00	2.04E+00	2.16E+00	-0.1202	1.43E+00	-0.0020
1	36	2.79E-28	4.34E-11	1.62E-11	3.86E-05	2.32E-05	6.68E-06	1.41E-02	1.12E-02	6.48E-03	2.08E-03	3.74E-02	4.09E-02	4.50E-02	4.19E-02	2.36E-02	5.97E-11	6.85E-05	3.39E-02	2.23E-01	1.00E+00	1.00E+00	9.73E-01	0.0266	1.05E+00	-0.0528
1.4	50.4	1.70E-40	9.62E-17	3.48E-17	2.33E-08	1.32E-08	3.41E-09	2.69E-04	1.94E-04	9.32E-05	2.29E-05	2.04E-02	1.78E-02	1.29E-02	7.03E-03	2.15E-03	1.31E-16	3.99E-08	5.79E-04	6.09E-02	7.14E-01	5.10E-01	5.46E-01	-0.0357	7.07E-01	0.0073
1.8	64.8	8.72E-53	1.49E-22	5.29E-23	7.79E-12	4.29E-12	1.04E-12	1.97E-06	1.35E-06	5.94E-07	1.28E-07	1.63E-03	1.31E-03	8.20E-04	3.59E-04	8.35E-05	2.02E-22	1.31E-11	4.04E-06	4.21E-03	5.56E-01	3.09E-01	3.64E-01	-0.0556	4.90E-01	0.0657
2.2	79.2	4.05E-65	1.88E-28	6.59E-29	1.86E-15	1.01E-15	2.35E-16	8.61E-09	5.77E-09	2.40E-09	4.75E-10	5.70E-05	4.41E-05	2.54E-05	9.84E-06	1.96E-06	2.54E-28	3.10E-15	1.73E-08	1.38E-04	4.55E-01	2.07E-01	2.47E-01	-0.0400	3.60E-01	0.0950
2.6	93.6	1.76E-77	2.06E-34	7.16E-35	3.56E-19	1.90E-19	4.34E-20	2.73E-11	1.79E-11	7.18E-12	1.35E-12	1.24E-06	9.30E-07	5.08E-07	1.82E-07	3.28E-08	2.77E-34	5.90E-19	5.38E-11	2.89E-06	3.85E-01	1.48E-01	1.62E-01	-0.0142	2.78E-01	0.1064
3	108	7.27E-90	2.04E-40	7.07E-41	5.85E-23	3.10E-23	6.94E-24	6.92E-14	4.49E-14	1.75E-14	3.17E-15	1.95E-08	1.44E-08	7.59E-09	2.58E-09	4.32E-10	2.75E-40	9.64E-23	1.35E-13	4.45E-08	3.33E-01	1.11E-01	1.07E-01	0.0043	2.36E-01	0.0973
3.6	129.6	1.81E-108	1.78E-49	6.10E-50	1.00E-28	5.25E-29	1.16E-29	6.59E-18	4.22E-18	1.60E-18	2.78E-19	2.58E-11	1.87E-11	9.47E-12	3.05E-12	4.73E-13	2.39E-49	1.64E-28	1.27E-17	5.74E-11	2.78E-01	7.72E-02	6.25E-02	0.0148	2.15E-01	0.0624
4	144	6.95E-121	1.51E-55	5.19E-56	1.30E-32	6.76E-33	1.47E-33	1.19E-20	7.57E-21	2.83E-21	4.82E-22	2.55E-13	1.83E-13	9.12E-14	2.85E-14	4.28E-15	2.03E-55	2.12E-32	2.28E-20	5.62E-13	2.50E-01	6.25E-02	4.81E-02	0.0144	2.13E-01	0.0375
4.5	162	2.04E-136	3.70E-63	1.27E-63	1.64E-37	8.50E-38	1.83E-38	3.92E-24	2.48E-24	9.16E-25	1.53E-25	6.76E-16	4.81E-16	2.35E-16	7.17E-17	1.04E-17	4.97E-63	2.67E-37	7.47E-24	1.47E-15	2.22E-01	4.94E-02	3.84E-02	0.0110	2.09E-01	0.0132
5	180	5.84E-152	8.62E-71	2.94E-71	1.91E-42	9.90E-43	2.12E-43	1.16E-27	7.30E-28	2.67E-28	4.37E-29	1.55E-18	1.10E-18	5.29E-19	1.58E-19	2.22E-20	1.16E-70	3.12E-42	2.20E-27	3.36E-18	2.00E-01	4.00E-02	3.28E-02	0.0072	2.01E-01	-0.0007
6	216	4.53E-183	4.16E-86	1.41E-86	2.20E-52	1.13E-52	2.39E-53	7.98E-35	4.97E-35	1.79E-35	2.86E-36	5.94E-24	4.16E-24	1.96E-24	5.68E-25	7.66E-26	5.57E-86	3.56E-52	1.50E-34	1.27E-23	1.67E-01	2.78E-02	2.52E-02	0.0026	1.71E-01	-0.0040
7.2	259.2	1.95E-220	1.50E-104	5.07E-105	2.07E-64	1.06E-64	2.22E-65	1.48E-43	9.19E-44	3.26E-44	5.13E-45	1.25E-30	8.69E-31	4.03E-31	1.14E-31	1.48E-32	2.01E-104	3.35E-64	2.78E-43	2.65E-30	1.39E-01	1.93E-02	1.77E-02	0.0016	1.32E-01	0.0067
8	288	2.33E-245	7.11E-117	2.40E-117	1.80E-72	9.17E-73	1.91E-73	1.96E-49	1.21E-49	4.27E-50	6.64E-51	3.72E-35	2.57E-35	1.18E-35	3.29E-36	4.23E-37	9.51E-117	2.91E-72	3.66E-49	7.84E-35	1.25E-01	1.56E-02	1.38E-02	0.0019	1.14E-01	0.0108
9	324	1.59E-276	2.64E-132	8.92E-133	1.38E-82	7.05E-83	1.46E-83	7.80E-57	4.80E-57	1.68E-57	2.59E-58	7.01E-41	4.83E-41	2.20E-41	6.06E-42	7.65E-43	3.54E-132	2.24E-82	1.45E-56	1.47E-40	1.11E-01	1.23E-02	1.02E-02	0.0021	1.01E-01	0.0100
10.8	388.8	0.00E+00	3.96E-160	1.33E-160	7.23E-101	3.67E-101	7.57E-102	2.92E-70	1.79E-70	6.22E-71	9.47E-72	2.54E-51	1.74E-51	7.85E-52	2.12E-52	2.62E-53	5.29E-160	1.17E-100	5.43E-70	5.30E-51	9.26E-02	8.57E-03	6.82E-03	0.0018	8.96E-02	0.0030
12	432	0.00E+00	1.05E-178	3.52E-179	4.25E-113	2.15E-113	4.43E-114	2.86E-79	1.75E-79	6.05E-80	9.15E-81	2.34E-58	1.60E-58	7.18E-59	1.93E-59	2.35E-60	1.40E-178	6.84E-113	5.31E-79	4.87E-58	8.33E-02	6.94E-03	5.58E-03	0.0014	8.23E-02	0.0011
14.4	518.4	0.00E+00	6.52E-216	2.19E-216	1.23E-137	6.23E-138	1.28E-138	2.17E-97	1.32E-97	4.55E-98	6.81E-99	1.48E-72	1.00E-72	4.47E-73	1.19E-73	1.43E-74	8.70E-216	1.98E-137	4.02E-97	3.06E-72	6.94E-02	4.82E-03	3.89E-03	0.0009	6.47E-02	0.0047
16	576	0.00E+00	9.59E-241	3.22E-241	4.90E-154	2.47E-154	5.05E-155	1.58E-109	9.63E-110	3.30E-110	4.92E-111	4.26E-82	2.89E-82	1.28E-82	3.38E-83	4.03E-84	1.28E-240	7.87E-154	2.92E-109	8.81E-82	6.25E-02	3.91E-03	3.11E-03	0.0008	5.52E-02	0.0073
18	648	0.00E+00	8.27E-272	2.78E-272	1.42E-174	7.16E-175	1.46E-175	9.51E-125	5.78E-125	1.97E-125	2.93E-126	4.38E-94	2.97E-94	1.31E-94	3.44E-95	4.07E-96	1.10E-271	2.28E-174	1.75E-124	9.05E-94	5.56E-02	3.09E-03	2.46E-03	0.0006	4.81E-02	0.0075
20	720	0.00E+00	6.79E-303	2.28E-303	3.82E-195	1.92E-195	3.91E-196	5.16E-140	3.13E-140	1.07E-140	1.58E-141	3.97E-106	2.68E-106	1.18E-106	3.08E-107	3.63E-108	9.06E-303	6.13E-195	9.52E-140	8.18E-106	5.00E-02	2.50E-03	2.06E-03	0.0004	4.39E-02	0.0061
25.2	907.2	0.00E+00	0.00E+00	0.00E+00	9.69E-249	4.88E-249	9.88E-250	7.44E-180	4.51E-180	1.53E-180	2.24E-181	1.24E-137	8.39E-138	3.68E-138	9.51E-139	1.10E-139	0.00E+00	1.56E-248	1.37E-179	2.56E-137	3.97E-02	1.57E-03	1.35E-03	0.0002	3.20E-02	0.0076
28	1008	0.00E+00	0.00E+00	0.00E+00	1.19E-277	6.01E-278	1.22E-278	2.25E-201	1.36E-201	4.60E-202	6.74E-203	1.11E-154	7.50E-155	3.28E-155	8.45E-156	9.77E-157	0.00E+00	1.92E-277	4.13E-201	2.29E-154	3.57E-02	1.28E-03	1.04E-03	0.0002	2.56E-02	0.0101
32	1152	0.00E+00	0.00E+00	0.00E+00	0.00E+00	0.00E+00	0.00E+00	3.54E-232	2.14E-232	7.23E-233	1.05E-233	4.14E-179	2.78E-179	1.21E-179	3.12E-180	3.59E-181	0.00E+00	0.00E+00	6.51E-232	8.48E-179	3.13E-02	9.77E-04	7.48E-04	0.0002	1.96E-02	0.0116
36	1296	0.00E+00	0.00E+00	0.00E+00	0.00E+00	0.00E+00	0.00E+00	4.91E-263	2.96E-263	1.00E-263	1.46E-264	1.31E-203	8.80E-204	3.83E-204	9.80E-205	1.12E-205	0.00E+00	0.00E+00	9.02E-263	2.68E-203	2.78E-02	7.72E-04	5.77E-04	0.0002	1.60E-02	0.0117
40	1440	0.00E+00	0.00E+00	0.00E+00	0.00E+00	0.00E+00	0.00E+00	6.16E-294	3.72E-294	1.25E-294	1.82E-295	3.66E-228	2.45E-228	1.07E-228	2.72E-229	3.11E-230	0.00E+00	0.00E+00	1.13E-293	7.48E-228	2.50E-02	6.25E-04	4.34E-04	0.0002	1.25E-02	0.0125
50.4	1814.4	0.00E+00	0.00E+00	0.00E+00	0.00E+00	0.00E+00	0.00E+00	0.00E+00	0.00E+00	0.00E+00	0.00E+00	3.41E-292	2.29E-292	9.91E-293	2.52E-293	2.86E-294	0.00E+00	0.00E+00	0.00E+00	6.97E-292	1.98E-02	3.94E-04	1.30E-04	0.0003	3.84E-03	0.0160

In Figure 1e, the log($a_N b_n$) was plotted against log(r) for the fitting of {N=-2..0,n//6} to the $|\vec{\mathbf{E}}| \propto 1/r^2$ curve. It showed a linear relationship. After a linear regression, the slope = -1.9943. When plotting log($1/r^2$) vs. log(r) for the $|\vec{\mathbf{E}}| \propto 1/r^2$ curve, it also showed a linear relationship with the slope = -2 (see Figure 1f). So, these two slopes are practically equal. Then, Figure 1e trigged me to develop a new "global fitting" method for fitting eq-2 to $|\vec{\mathbf{E}}| \propto 1/r^2$ curve.

I-b. "Global fitting" of eq-2 to $|\vec{\mathbf{E}}| \propto 1/r^2$

From the undergraduate course (~ 40 years ago), I learned that for an exponential curve, if appropriately cut it into three segments (along x-axis), and then re-scale the y-scale of these three segments appropriately, we will obtain three

(apparently) exactly same shaped curves (note: it can be seen more straightforward in the linearized log(exp) plotting). Based on the preliminary fitting result in Figure 1e, I realized that we maybe can do the same trick in the fitting of Figure 1d. Eq-2 already naturally segregated r-1D into many N super shells. We only need to fix the values of $b_1 \sim b_5$ as one set, and then use the same (fixed) $b_1 \sim b_5$ values for each of all N super shells, and then re-scale the y-axis appropriately by adjusting the coefficient a_N in eq-2.

In Table 3 (columns 1 ~ 10) and Figure 2, I successfully applied this idea in the fitting of four N super shells to the $|\vec{\mathbf{E}}| \propto 1/r^2$ curve. Here is the brief explanation on how it works. In Table 3, from the relative r (or r/r_1 =1, 4, 9, 16, 25, see column 2) of each of the four N super shells (see column 1), we first calculated out the real r values (see column 4) by using the standard {N,n//6} QM method (see column 3). Then, we calculated out the $1/r^2$ curve values (see column 6) and used it as the template curve for the fitting. In column 7, according to the previous results (see Table 1, Table 2, etc.), I first assumed the initial values for $a_{N=-3}$, $a_{N=-2}$, $a_{N=-1}$, and $a_{N=0}$, and then used them to divided the template $1/r^2$ curve in column 6 (note: need to match the right color for each cell in the spread sheet). Then, the "global fitting" was done by manually and repetitively adjusting the values of $a_{N=-3}$ through $a_{N=0}$, until the four sets of $b_1 \sim b_5$ values become exactly the same (see column 7). (Note: After many tries, I realized that there is a relationship of $a_{N=-3} = 36^2 \times a_{N=-2} = 36^2 \times 36^2 \times a_{N=-1} = 36^2 \times 36^2 \times 36^2 \times a_{N=0}$). The final result obtained was: $b_1 = 1296$, $b_2 = 81$, $b_3 = 16$, $b_4 \approx 5.06$, $b_5 \approx 2.07$, and this set of $b_1 \sim b_5$ values were fixed for all four N super shells of {N=-3..0,n//6} fitting curve (see the column 7 in Table 3). The y-axis re-scaling factors were manually adjusted to be: $a_{N=-3} \approx 1679616$, $a_{N=-2} \approx 1679616 / 36\text{^}2 \approx 1296$, $a_{N=-1} \approx 1679616 / 36\text{^}4 \approx 1$, $a_{N=-1} \approx 1679616 / 36\text{^}6 \approx 0.0007716$, (see the column 7 in Table 3). I called this method as the "Global Fitting". In Figure 2a, when we plotted the $\log(a_N b_n)$ vs. log(r), (i.e., column 10 vs. column 5), it showed a perfect linear relationship with a slop = -2 exactly. This slope is exactly the same as that for log(1/r^2) vs. log(r) plot (as shown in Figure 1f). Then, in Figure 2b, we put this set of $b_1 \sim b_5$ (fixed values) and $a_{N=0}$ into Table 1 (that using a single super shell of {0,n//6} to fit to $|\vec{\mathbf{E}}| \propto 1/r^2$ curve), it fitted quite well (within the range of $1 \le r \le 36$). In Figure 2c, we put this set of $b_1 \sim b_5$ (fixed values) and $a_{N=0}$ and $a_{N=-1}$ into Table 2 (that using two super shells of {N=-1..0,n//6} to fit to $|\vec{\mathbf{E}}| \propto 1/r^2$ curve), it fitted reasonably well (within the range of $\frac{1}{36} \le r \le 36$). In Figure 2d, we put this set of $b_1 \sim b_5$ (fixed values) and $a_{N=-2..0}$ into a three super shells of {N=-2..0,n//6} to fit to $|\vec{\mathbf{E}}| \propto 1/r^2$ curve, it fitted reasonably well (within the range of $\frac{1}{36^2} \le r \le 36$). In Figure 2e, we put this set of $b_1 \sim b_5$ (fixed values) and $a_{N=-3..0}$ into a four super shells of {N=-3..0,n//6} to fit to $|\vec{\mathbf{E}}| \propto 1/r^2$ curve, it fitted reasonably well (within the range of $\frac{1}{36^3} \le r \le 36$). Under the eq-2, the real equation for Figure 3a and figure 3e is shown in eq-5 below

$$\sum_{N=-3}^{N=0} a_N \left[\sum_{n=1}^{n=5} b_n {r_N}^2 |R(n,l)|^2 \right] =$$

$$36^4 \times [1296\, {r_{N=-3}}^2 |R(1,0)|^2 + 81\, {r_{N=-3}}^2 |R(2,l)|^2 + 16\, {r_{N=-3}}^2 |R(3,l)|^2 + 5.06\, {r_{N=-3}}^2 |R(4,l)|^2 + 2.07\, {r_{N=-3}}^2 |R(5,l)|^2] +$$
$$36^2 \times [1296\, {r_{N=-2}}^2 |R(1,0)|^2 + 81\, {r_{N=-2}}^2 |R(2,l)|^2 + 16\, {r_{N=-2}}^2 |R(3,l)|^2 + 5.06\, {r_{N=-2}}^2 |R(4,l)|^2 + 2.07\, {r_{N=-2}}^2 |R(5,l)|^2] +$$
$$36^0 \times [1296\, {r_{N=-1}}^2 |R(1,0)|^2 + 81\, {r_{N=-1}}^2 |R(2,l)|^2 + 16\, {r_{N=-1}}^2 |R(3,l)|^2 + 5.06\, {r_{N=-1}}^2 |R(4,l)|^2 + 2.07\, {r_{N=-1}}^2 |R(5,l)|^2] +$$
$$36^{-2} \times [1296\, {r_{N=0}}^2 |R(1,0)|^2 + 81\, {r_{N=0}}^2 |R(2,l)|^2 + 16\, {r_{N=0}}^2 |R(3,l)|^2 + 5.06\, {r_{N=0}}^2 |R(4,l)|^2 + 2.07\, {r_{N=0}}^2 |R(5,l)|^2]$$

eq-5

(Note: It seems that there is always some under-fitting (at the small r side) in the global fitted curves in Figure 2 (c, d, e), and it is normal. This under-fitting will be filled-in if we add more and more N super shells for the fitting. In contrast, the manually fitted curve (see Figure 1 (c, d)) seems more perfect (at the smaller r side) than that of the global fitted curves (see Figure 2 (c, d, e)), but actually they are over-fitted. This over-fitting left no room for adding more N super shells for the better fitting at the smaller r side. Therefore, the global fitting is always better than the manual fitting, and the global fitting will become a perfect fitting once we increased the N super shell numbers to $-\infty < N < \infty$).

Table 3. A global fitting of eq-2 that used four N super shells {N=-3..0,n//6} to fit to $|\vec{\mathbf{E}}| \propto 1/r^2$ curve.

					global fitting to E					global fitting to U				
						dev. (=a_N)					dev. (=a_N)			
					$a_{N=-3}$ =	1679616				$a_{N=-3}$ =	1296			
					$a_{N=-2}$ =	1296	1296			$a_{N=-2}$ =	36	36		
					$a_{N=-1}$ =	1	1296			$a_{N=-1}$ =	1	36		
					$a_{N=0}$ =	0.000772	1296			$a_{N=0}$ =	0.027778	36		
N =	relative r =	(real) r =	real r_n = r/36^x	log(r_n)	1/r^2	raw $b_1 \sim b_5$	check (b1~b5)*r^2	$a_N b_n$ =	log($a_N b_i$)	1/r	raw b_n	check (b1~b5)*r	$a_N b_n$ =	log($a_N b_i$)
-3	1	r/36^3	2.14E-05	-4.66891	2.18E+09	1296.00	1296	2.18E+09	9.337815	46656	36.00	36	46656	4.668908
	4	r/36^3	8.57E-05	-4.06685	1.36E+08	81.00	1296	1.36E+08	8.133695	11664	9.00	36	11664	4.066848
	9	r/36^3	0.000193	-3.71466	2.69E+07	16.00	1296	2.69E+07	7.42933	5184	4.00	36	5184	3.714665
	16	r/36^3	0.000343	-3.46479	8.50E+06	5.06	1296	8.50E+06	6.929575	2916	2.25	36	2916	3.464788
	25	r/36^3	0.000536	-3.27097	3.48E+06	2.07	1296	3.48E+06	6.541935	1866.24	1.44	36	1866.24	3.270967
-2	1	r/36^2	0.000772	-3.11261	1.68E+06	1296.00	1296	1.68E+06	6.22521	1296	36.00	36	1296	3.112605
	4	r/36^2	0.003086	-2.51055	1.05E+05	81.00	1296	1.05E+05	5.02109	324	9.00	36	324	2.510545
	9	r/36^2	0.006944	-2.15836	2.07E+04	16.00	1296	2.07E+04	4.316725	144	4.00	36	144	2.158362
	16	r/36^2	0.012346	-1.90849	6.56E+03	5.06	1296	6.56E+03	3.81697	81	2.25	36	81	1.908485
	25	r/36^2	0.01929	-1.71466	2.69E+03	2.07	1296	2.69E+03	3.42933	51.84	1.44	36	51.84	1.714665
-1	1	r/36	0.027778	-1.5563	1296	1296.00	1296	1296	3.112605	36	36.00	36	36	1.556303
	4	r/36	0.111111	-0.95424	81	81.00	1296	81	1.908485	9	9.00	36	9	0.954243
	9	r/36	0.25	-0.60206	16	16.00	1296	16	1.20412	4	4.00	36	4	0.60206
	16	r/36	0.444444	-0.35218	5.0625	5.06	1296	5.0625	0.704365	2.25	2.25	36	2.25	0.352183
	25	r/36	0.694444	-0.15836	2.0736	2.07	1296	2.0736	0.316725	1.44	1.44	36	1.44	0.158362
0	1	r	1	0	1	1296.00	1296	1	0	1	36.00	36	1	0
	4	r	4	0.60206	0.0625	81.00	1296	0.0625	-1.20412	0.25	9.00	36	0.25	-0.60206
	9	r	9	0.954243	0.01235	16.00	1296	0.012346	-1.90849	0.111111	4.00	36	0.111111	-0.95424
	16	r	16	1.20412	0.00391	5.06	1296	0.003906	-2.40824	0.0625	2.25	36	0.0625	-1.20412
	25	r	25	1.39794	0.0016	2.07	1296	0.0016	-2.79588	0.04	1.44	36	0.04	-1.39794

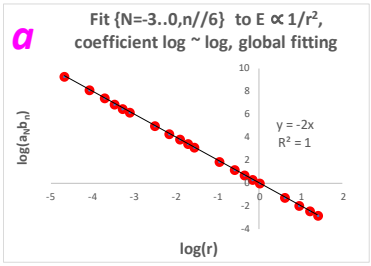

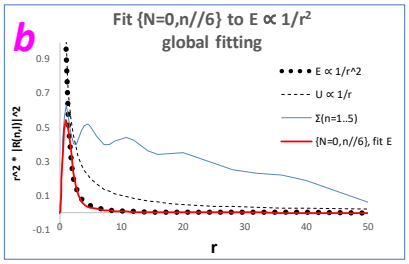

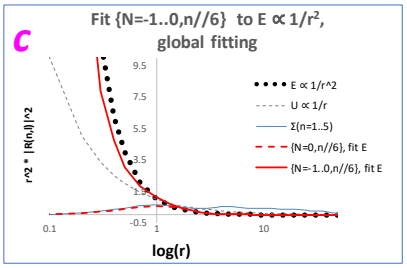

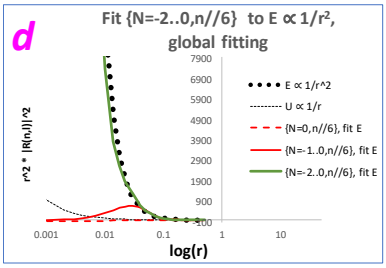

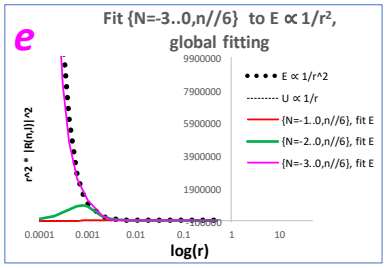

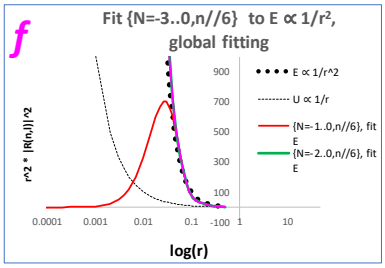

Figure 2a. Global fitting of eq-2 with four N super shells {N=-3..1,n//6} to fit to $|\vec{\mathbf{E}}| \propto 1/r^2$ curve, the coefficient $a_N b_n$ plot (see the red dots). The black solid line is the linear regression.

Figure 2b. Global fitting of eq-2 with a single N super shell {0,n//6} QM to fit to $|\vec{\mathbf{E}}| \propto 1/r^2$ curve (see the red solid-line curve vs. the black dotted curve).

Figure 2c. Global fitting of eq-2 with two N super shells {N=-1..0,n//6} to fit to $|\vec{\mathbf{E}}| \propto 1/r^2$ curve (see the red solid-line curve vs. the black dotted curve).

Figure 2d. Global fitting of eq-2 with three N super shells {N=-2..0,n//6} QM to fit to $|\vec{\mathbf{E}}| \propto 1/r^2$ curve (see the green solid-line curve vs. the black dotted curve).

Figure 2e. Global fitting of eq-2 with four N super shells {N=-3..0,n//6} QM to fit to $|\vec{\mathbf{E}}| \propto 1/r^2$ curve (see the pink solid-line curve vs. the black dotted curve).
Figure 2f. Same as Figure 2e except that y-axis was scaled down to 1/10000.

I-c. Global fitting of eq-2 to U ∝ 1/r

The exact same method can also be used to reconstitute (or to fit) the electric potential U ∝ 1/r curve for the range of $0 < r < \infty$ (by using the Born probability's r-1D distribution function). Column 25 ~ 27 in Table 1 showed the single N = 0 super shell (manually) fitted data, and column 26 ~ 28 in Table 2 showed the N = -1..0 two super shells manually fitted data, and column 11 ~ 15 in Table 3 showed the four super shells {N=-3..0,n//6} global fitted data (all fit to U ∝ 1/r). From now on, we are interested only in the global fitting. Table 3 showed the global fitting result of $b_1 = 36$, $b_2 = 9$, $b_3 = 4$, $b_4 \approx 2.25$, $b_5 \approx 1.44$, and they were fixed for each of all four N super shells of {N=-3..0,n//6} fitting curve (see the column 12 in Table 3). The y-axis re-scaling factors were manually adjusted to be: $a_{N=-3} = 1296$, $a_{N=-2} = 1296 / 36 = 36$, $a_{N=-1} = 1296 / 36\text{^}2 = 1$, $a_{N=0} = 1296 / 36\text{^}3 \approx 0.0278$, (see the column 12 in Table 3).

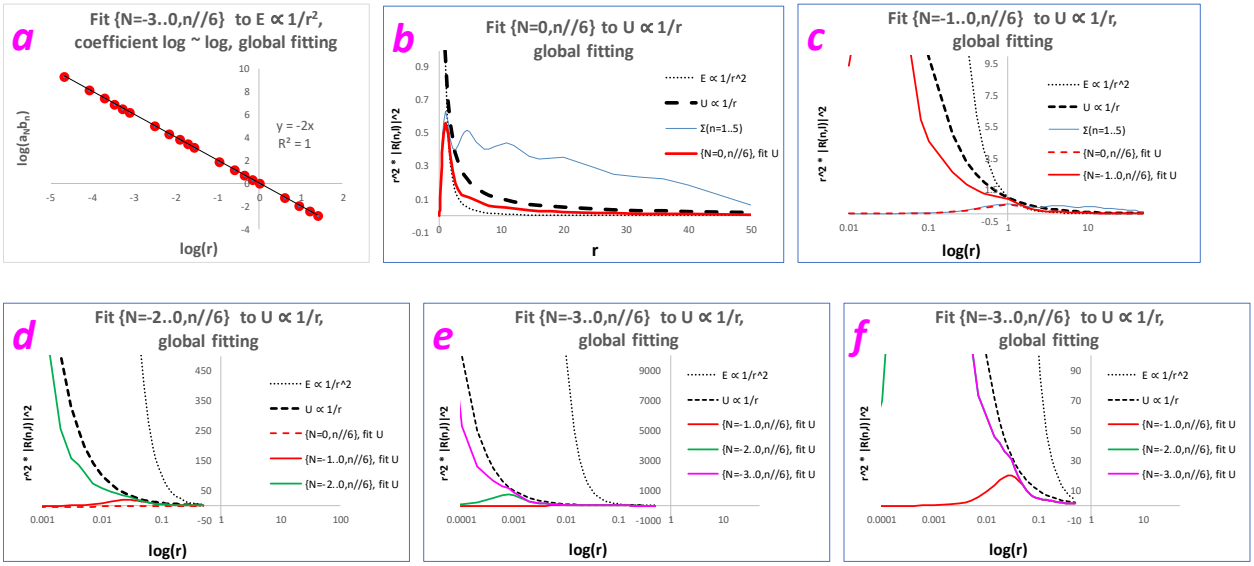

Figure 3a. Global fitting of eq-2 with four N super shells {N=-3..1,n//6} to fit to U ∝ 1/r curve, the coefficient $a_N b_n$ plot (see the red dots). The black solid line is the linear regression.
Figure 3b. Global fitting of eq-2 with a single N super shell {0,n//6} QM to fit to U ∝ 1/r curve (see the red solid-line curve vs. the black dash-line curve). For the blue solid-line, it was eq-2 with $a_N b_n \equiv 1$ (see SunQM-6's Fig-9a).
Figure 3c. Global fitting of eq-2 with two N super shells {N=-1..0,n//6} to fit to U ∝ 1/r curve (see the red solid-line curve vs. the black dash-line curve).
Figure 3d. Global fitting of eq-2 with three N super shells {N=-2..0,n//6} QM to fit to U ∝ 1/r curve (see the green solid-line curve vs. the black dash-line curve).
Figure 3e. Global fitting of eq-2 with four N super shells {N=-3..0,n//6} QM to fit to U ∝ 1/r curve (see the pink solid-line curve vs. the black dash-line curve).
Figure 3f. Same as Figure 2e except that y-axis was scaled down to 1/100.

In Figure 3a, when we plotted the $\log(a_N b_n)$ vs. $\log(r)$, (see column 15 vs. column 5 in Table 3), it showed a perfect linear relationship with a slop = -1. This slope is exactly the same as that for log(1/r) vs. log(r) plot (as shown in Figure 1f). Then, in Figure 3b, we used this set of the (fixed) $b_1 \sim b_5$ values and $a_{N=0}$ value to fit to (or to reconstitute) $U \propto 1/r$ curve (by using a single super shell of {0,n//6}), it fitted reasonably well (within the range of $1 \le r \le 36$). In Figure 3c, we used this set of the (fixed) $b_1 \sim b_5$ values and $a_{N=-1..0}$ values to fit to $U \propto 1/r$ curve (by using two super shell of {N=-1..0,n//6}), it fitted reasonably well (within the range of $\frac{1}{36} \le r \le 36$). In Figure 3d, we used this set of the (fixed) $b_1 \sim b_5$ values and $a_{N=-2..0}$ values to fit to $U \propto 1/r$ curve (by using three super shell of {N=-2..0,n//6}), it fitted reasonably well (within the range of $\frac{1}{36^2} \le r \le 36$). In Figure 3e, we used this set of the (fixed) $b_1 \sim b_5$ values and $a_{N=-3..0}$ values to fit to (or to reconstitute) $U \propto 1/r$ curve (by using four super shell of {N=-3..0,n//6}), it fitted reasonably well (within the range of $\frac{1}{36^3} \le r \le 36$).

Comparing Figure 3 with Figure 2, it was obvious that the fitting for $U \propto 1/r$ curve was significantly poor (or significantly under-fit) than the fitting for $E \propto 1/r^2$ curve (e.g., see the green line curves in Figure 3d vs. in Figure 2d). It means that when using eq-2 to fit to $E \propto 1/r^2$ curve for the {-1,n//6} range, (i.e., for the range of $\frac{1}{36} \le r \le 1$), we may only need to use three super shells, or $\Delta N = 3$, or{N=-2..0,n//6}, to fit and it will get a reasonably good fitting. But when using eq-2 to fit to $U \propto 1/r$ curve for the same {-1,n//6} range, (i.e., also for the range of $\frac{1}{36} \le r \le 1$), we may have to use seven super shells, or $\Delta N = 7$, or{N=-4..2,n//6}, to fit to get the same quality of fitting. This further means, if we treat eq-2 as a mathematical series (like Tayler Series), it has a (relative) good convergence for the $1/r^2$ curve reconstitution, and it has a (relative) poor convergence for the 1/r curve reconstitution.

Furthermore, when comparing Figure 3f with Figure 2f, we see that the fitting curve for $U \propto 1/r$ is much bumpier than the fitting curve for $E \propto 1/r^2$. Besides that it may needs many more N super shells to improve the fitting for 1/r, there may be a second explanation for it. According to the above QM analysis, we may can say that under the wave mechanics (of QM), both electric field and the potential field are (truly? or not truly?) composed by the Schrodinger equation/solution's radial wave functions. While a single point charge's static electric field does behave exactly (or nearly exactly) like the classical physics' $|\vec{\mathbf{E}}| \propto 1/r^2$ curve (or, has its strength smoothly decrease vs. r), its potential field may have some significant quantum effect (in comparison with the classical physics' $U \propto 1/r$ smooth curve). Its strength may have a noticeable quantum drop (besides the general 1/r smooth decreasing) at the out edge of each super shell of its {N,n//q} QM. And its strength may even have a less noticeable quantum drop at the out edge of each n shell (within each single super shell of its{N,n//q} QM). In other words, the classical physics $|\vec{\mathbf{E}}| \propto 1/r^2$ curve may describe the true electric field with high accuracy, while the classical physics $U \propto 1/r$ curve may only describe the true electric potential field with approximation. If this hypothesis is correct, then the quantum effect of the proton's electric potential may have made the significant contribution to a H-atom's electron orbital configuration. Also, the quantum effect of our Sun's gravitational potential may have made the significant contribution to the eight planets' orbital configuration in our solar system. In other words, is it possible that a potential field is more towards to a true quantum field, not exactly a 1/r smooth field?

I-d. A complete global fitting in {N,n//q} QM (with its Born probability density) may can be used to reconstitute any point-centered field

Because the global fitting will produce a perfect fitting once we increased the N super shell numbers to $-\infty < N < \infty$, therefore, from the result of section I-b, the formula of eq-2 can be re-written as a true equation as

$$\sum_{N\to-\infty}^{N\to\infty} a_N \left[\sum_{n=1}^{n=5} b_n {r_N}^2 |R(n,l)|^2\right] = \frac{1}{r^2} \qquad \text{eq-6}$$

Then, times $\frac{q}{4\pi\epsilon_0}$ on the both sides in eq-6, we will have

$$\frac{q}{4\pi\epsilon_0}\sum_{N\to-\infty}^{N\to\infty} a_N \left[\sum_{n=1}^{n=5} b_n {r_N}^2 |R(n,l)|^2\right] = \frac{q}{4\pi\epsilon_0}\frac{1}{r^2} = \left|\vec{\mathbf{E}}\right| \qquad \text{eq-7}$$

(Note: To balance the physical unit at the two sides of eq-7, the coefficient b_n in eq-7 should have a physical unit of 1/r). Similarly, from the result of section I-b, eq-2 can also be re-written as a true equation as

$$\sum_{N\to-\infty}^{N\to\infty} a_N \left[\sum_{n=1}^{n=5} b_n {r_N}^2 |R(n,l)|^2\right] = \frac{1}{r} \qquad \text{eq-8}$$

Times $\frac{q}{4\pi\epsilon_0}$ on the both sides in eq-8, we will have

$$\frac{q}{4\pi\epsilon_0}\sum_{N\to-\infty}^{N\to\infty} a_N \left[\sum_{n=1}^{n=5} b_n {r_N}^2 |R(n,l)|^2\right] = \frac{q}{4\pi\epsilon_0}\frac{1}{r} = |U| \qquad \text{eq-9}$$

(Note: To balance the physical unit at the two sides of eq-9, the coefficient b_n in eq-9 should have a physical unit of zero). Both eq-7 and eq-9 formally confirmed that (the Coulomb Law based) electric field formula (and the electric potential formula) can be reconstituted by using the {N,n//6} QM structure, that is, by using the Born (radial) probability function.

This result reminded me that what I had learned in my undergraduate courses (over 40 years ago): the Tayler series [28], the Fourier series [28], the Hilbert space that have the infinite vector basis for the infinite dimensions, etc. [29]. (But sorry, I already forgot almost all of them because since then I became a biophysicist for over 30 years). With $a_N b_n$ determined under the global fitting, the radial Born probability density function in the eq-2 become a normalized mathematical series, or a series of the unit vector bases in the (high dimensional) Hilbert space, that can be used to reconstitute any point-centered field (e.g., the force field, the potential field, the mass field, etc.) with 1/r^x function (where x can be any integer like 1, 2, …, or can be any real number like 3.297, 2.33, 0.5, etc.). Furthermore, this conclusion can be extended to a general {N,n//q} QM (where q can be any integer number that greater than 1, not only limited to q = 6): a complete global fitting in {N,n//q} QM (with its Born probability density) can be used to reconstitute any point-centered field.

Some of the well-known point-centered fields includes: a single point charge's static electric field strength $E = \frac{q}{4\pi\epsilon_0}\frac{1}{r^2}$ and its potential field $U = -\frac{1}{4\pi\epsilon_0}\frac{e^2}{r}$, two charges (Q and q)'s Coulomb force field $F = \frac{1}{4\pi\epsilon_0}\frac{Qq}{r^2}$, Newton's law of universal gravitation (between two objects M and m) $F = G\frac{Mm}{r^2}$ and its potential field $U = -G\frac{Mm}{r}$, the (roughly) estimated mass (density radial distribution) field inside the Sun, $D \approx 1.26 \times 10^{23}\frac{1}{r^{2.33}}$ (kg/m^3), (see SunQM-3's eq-17), and the (roughly) estimated mass (density radial distribution) field in Solar system's {N=3..4,n=1..5//6}o region, $D \approx 4.37 \times 10^{28}\frac{1}{r^{3.279}}$ (kg/m^3), (see SunQM-1s1's Table 3b. Remember that I had used it to estimate the original mass not only for all eight known planets, but also for the four undiscovered planets {3,2}, {3,3}, {3,4} and {3,5}).

It is interesting to see that this method had been used in my early SunQM papers (even I did not fully understand it at that time): in SunQM-3's Fig-3b, I used D(r) * $\sum_{N=0}^{N=-2}\left[\sum_{n=1}^{n=5} {r_N}^2 |R(n,l)|^2\right]$, (where D(r) is the mass density inside the Sun), to plot Sun's radial mass distribution (inside the Sun). It actually is to use D(r) to modulate the amplitude of each $r^2|R(n,l)|^2$. In that case, the function of D(r) is equivalent to the coefficient of $a_N b_n$ in the eq-2.

When I proposed that we should be able to use Schrodinger equation/solution to describe the E/RFe-force field (see SunQM-6's eq-1), there were two major (conceptual) obstacles (at least for me). The first (and most important) obstacle was, we need to give one real example to show how to do it, and here we showed one real example (with eq-7 and eq-9). The second obstacle was, the traditional Schrodinger equation/solution is always explained as the Born probability density distribution (in a steady QM state), which is conceptually different than either the force field, or the trajectory of a motion of an object. Now with the new concept of NPB (see SunQM-4s1), and with the re-explanation of the Born probability 3D density distribution as the collection of all orbital tracks (see SunQM-6s2's Fig-1 through Fig-5), and with the 3D wave packet description and the dis-entanglement of the outmost shell (or the "general decaying" process, see SunQM-6s1, -6s2, -6s3, etc.), the "|nL0> elliptical/parabolic/hyperbolic orbital transition model" (see SunQM-6s2, -6s3), this problem has also been solved. So, by now, I am 100% sure that the E/RFe-force field (and also the G/RFg-force field) do can be described by Schrodinger equation/solution. The next question is, is the eq-7 the simplest (analytical?) formula that using Schrodinger

equation/solution to represent a single point charge's static electric field strength $E = \frac{q}{4\pi\epsilon_0}\frac{1}{r^2}$? In other words, is there any formula (or equation) that is simpler (or more analytical, or better) than the eq-7 for this purpose?

In SunQM-3s8's Fig-1b, when using $D(r) * \sum_{N=0}^{N=-1}[\sum_{n=1}^{n=5} r_N{}^2|R(n,l)|^2]$ to mimic Sun's radial mass density r-distribution, we saw that the curve had some bumps on top of a smooth declining curve ($D = A/r^B - C$), and we explained the bumpiness as the quantum change of the mass in the r-1D distribution (something equivalent to the "planetary differentiation"). Based on this result, here I guess that even the real electric field strength $|\vec{\mathbf{E}}(r)|$ maybe is not completely as smooth as the $1/r^2$ curve, and it may also have some (minor or unnoticeable) quantum drop as r increasing. However, our fitting result (by using eq-2) is too preliminary to show any result on this issue.

II. Alternatively, we may can use the traditional QM to fit to $|\vec{\mathbf{E}}| \propto 1/r^2$, although the r_1 has to be moved inward infinitely (according to the concept from the {N,n} QM)

In the college, I learned that in the Fourier transformation, because the sine functions (with all frequencies) formed a complete set of basis for the 1D space in a frequency domain, the combination of many sine waves with the appropriate frequencies and amplitudes can fit to any 1D (odd functional) shaped curve in the time domain. While working on this paper, I realized that all the radial wave functions (from n=1 to n=∞) of a H-atom's Schrodinger equation/solution (or the Born probability's radial density function) maybe formed a complete set of basis for a point-centered spherical space (or, for the r-1D space with $n \gtrapprox 1$), so that we should be able to use these whole set of r-1D basis (with the appropriate amplitudes, see eq-10) to reconstitute any point-centered field (including the force field and its potential field, and any point-centered mass distribution) function in the r-1D space. (Note: Maybe Hilbert (or other scientists) already explained the exact same idea ~100 years ago. If so, readers please let me know. Sorry, I am a citizen scientist, don't familiar with the history of the Hilbert space theory).

$$\sum_{n=1}^{n=\infty} b_n\, r^2|R(n,l)|^2 \qquad \text{eq-10}$$

The key difference between eq-2 and eq-10 is: in eq-2, we used many (or infinite number of) N super shells (and each N super shell contains only finite number of n shells) to cover the r-1D space (from r = 0 to r = ∞), while in eq-10, we used a single N super shell (that contains infinity number n shells) to cover the r-1D space (from r = 1 to r = ∞). For the r-1D space with n < 1, we can use {N,n//q} QM's (unusual) property to move the r_1 inward, that is, to use the high frequency n', to fit. (Note: for how to move the r_1 inward, see either SunQM-3s11's Table 1, or SunQM-5s2's Table 4). So, in eq-10, n can be the base frequency n, but usually, it is the high-frequency n'. For example, to use eq-10 to describe a proton's electric field in the H-atom, based on the {N,n//6} QM, we can move the r_1 (usually is the Bohr radius a_0 = 5.29E-11 meters) inward to $r_1 = r_{proton}$ = 8.4E-16 meters.

From Figure 1a, we know that for the small n number (like $1 \leq n < 10$), the curve of eq-10 shows more bumpiness (e.g., see the blue line curve of Figure 1b (for $b_n \equiv 1$ in eq-10)), and for the large n number (or the high-frequency n'), the curve of eq-10 shows almost no bump (or completely no bump). In other words, if we see a r-1D curve (of one physical property) has bumps, it must reflect that this physical property in a strong quantum (mechanical) state (i.e., with n < 10), and if we see a r-1D curve (of one physical property) has no bumps, it must reflect that this physical property in a classical (mechanical) state (i.e., with n >> 10). For example, at high n', the quantum effect is faded out to be the classical-like $|\vec{\mathbf{E}}| = \frac{q}{4\pi\varepsilon_0}\frac{1}{r^2}$ equation. So, we may can directly write down the true equation of

$$\sum_{n=1}^{n=\infty} b_n r^2|R(n,l)|^2 = |\vec{\mathbf{E}}| = \frac{q}{4\pi\varepsilon_0}\frac{1}{r^2} \qquad \text{eq-11}$$

Furthermore, in eq-11, we may can define

$$b_n = b'_n \frac{q}{4\pi\varepsilon_0}\frac{1}{r^2} \qquad \text{eq-12}$$

(Note: Since b_n has the unit of 1/r, b'_n must have a unit of r). Put eq-12 into eq-11, we have

$$\sum_{n=1}^{n=\infty} b'_n \frac{q}{4\pi\varepsilon_0}\frac{1}{r^2}[r^2|R(n,l)|^2] = \frac{q}{4\pi\varepsilon_0}\frac{1}{r^2} \qquad \text{eq-13}$$

or,

$$\sum_{n=1}^{n=\infty} b'_n[r^2|R(n,l)|^2] = 1, \text{ (within } 0 < r < \infty) \qquad \text{eq-14}$$

(Note: eq-14 has a zero physical unit). In eq-14, each $\sum_{n=1}^{n=\infty} b'_n[r^2|R(n,l)|^2] = 1$ function (at each n) becomes a unitary vector base (note: ideally it should be only within each Δr space of $r_n \le r < r_{n+1}$, however, in reality, it is within $0 < r < \infty$), and all of them formed a complete set of unitary vector bases for a Hilbert space (for the reconstitution of the electric field $|\vec{\mathbf{E}}| = \frac{q}{4\pi\varepsilon_0}\frac{1}{r^2}$ curve in a Hilbert space of r_n with vector bases from $r_{n=1}$, $r_{n=2}$, $r_{n=3}$, up to $r_{n=\infty}$). (Note: Therefore, the function of $b'_n[r^2|R(n,l)|^2]$ is not a "good" function to work as a unit vector base, because it spreads to its neighboring unit vector bases. Also see section III for more explanations).

Then, can we check this method by showing one example? The answer is "No" for me, because it needs to know the H-atom's radial wave function R(n,l) not only for n > 5, but also for n in extremely large number (e.g., 6^9, 6^9 +1, etc.), and I am not able to obtain those R(n,l) functions.

If using eq-10, we only see the recognizable QM effect in the near-center distance range from n = 1 to n < 10, while in the far distance range (i.e., n >> 10), the QM process will fade away and become a continuous process. For example, when describing a proton's electric field in an H-atom by using eq-10 (and ignoring the eq-2) with $r_1 = r_{proton}$ = 8.4E-16 meters, we may see the quantum effect only at n < 10 (i.e., at the r that just outside the proton surface), we will unable to see (or to recognize) the (high level) quantum effect at n ≈ 6^3, (i.e., at the r that around the Bohr radius a_0 = 5.29E-11 meters). In contrast, if using eq-2, it tells us that the above saying is only correct within a single super shell (i.e., within ΔN = 1). If we increased distance range far enough (e.g., ΔN > 2), we always can find another level of QM effect. The eq-2 showed that the extra (higher level) quantum effect of N super shells is always there, and it only can be seen under the condition that 1) not only the range of viewing has to be larger than several N super shells; 2) but also the scale of viewing has to be large enough (i.e., must be based on N super shell). That is why we always use the eq-2 as the primary method for the quantum description, and eq-10 is (mostly) good for the classical process description. In this sense, eq-2 shows more on the quantum side, while eq-10 shows more on the continue side. From this point of view, or from the view of the wave mechanics, any point-centered force (or field, or the mass distribution) that can be constituted as the collection of rθφ-3D radial waves, if viewed in a large enough scale, we will see that it (always) has the intrinsic quantum change character (from the top-down view). Meanwhile, if viewed in a small scale, we will see that it only shows the apparent continues change character (from the bottom-up view).

This discussion turned my previous physical concept up-side-down. Before the discovery of {N,n} QM, I believed that the continues change is the foundation of physics, and the quantum effect is the special case in physics, (or the "continuous" is the absolute, the "quantum" is the relative). After {N,n} QM and after this discussion, now I start to believe that the quantum effect is the foundation of physics, and the continues change is the trivial case in physics, (or the "quantum" is the absolute, the "continuous" is the relative).

III. Using {N,n//2^j} QM structure's radial Born probability to constitute the Earth's radial mass density curve

Figure 4a showed the Earth's true mass density D(r) curve. Now we try to use Schrodinger equation/solution (or Born probability) to reconstitute it. The easiest way is to use eq-10 (or eq-11) kind of method:

$\sum_{n=1}^{n=\infty} b_n r^2 |R(n,l)|^2 = \mathrm{D(r)}$ eq-15

with

$b_n = b'_n \, \mathrm{D(r)}$ eq-16

(Note: by ignoring the mass unit and only consider the distance unit, D(r) has a unit of 1/r^3, b_n has a unit of 1/r^2, and b'_n has a unit of r). So that

$\sum_{n=1}^{n=\infty} \mathrm{D(r)} \; b'_n [r^2 |R(n,l)|^2] = \mathrm{D(r)}$ eq-17

and

$\sum_{n=1}^{n=\infty} b'_n [r^2 |R(n,l)|^2] = 1$, (within $0 < r < \infty$) eq-18

Then, in eq-18, each $\sum_{n=1}^{n=\infty} b'_n [r^2 |R(n,l)|^2] = 1$ function becomes a unitary vector base (ideally should be only within each Δr space of $r_n \le r < r_{n+1}$, however, in reality, it is within $0 < r < \infty$), and all of them formed a complete set of unitary vector bases for a Hilbert space (for the reconstitution of the Earth's mass density D(r) curve in a Hilbert space of r_n with vector bases from $r_{n=1}$, $r_{n=2}$, $r_{n=3}$, up to $r_{n=\infty}$). (Note: For eq-17 and eq-18, we may can use integration to replace the sum, and change the range from $1 \le n \le \infty$, to, $r_1 < r \le \infty$ (by using $r_n = r_1 * n\text{^}2$)).

However, there is a shortcoming for eq-17: it is a curve fitting for the classical process (or the continuous curve), because its "unit vector base function" does not provide any information on the Earth's {N,n//2} quantum structure. Then, how to increase the Earth's {N,n//2} quantum structure information in eq-17? Or, the more correct way to ask this question is, how to add the Earth's {N,n//2} quantum structure information in the "unit vector base functions" of eq-17?

Here we showed one possible way. First, in eq-17, instead of summing from n=1 to n=∞, let's simplify the sum to be from n=1 to n= 256. (Note: Why we choose n = 256 = 2^8? It is because that based on {N,n//q} QM, Earth primarily belongs to a {N,n//2} QM structure, and it gives the inner core of the Earth has a radius $(½)^2 = ¼$ of the Earth's radius (see SunQM-1s3); Besides that, Earth also belongs to a {N,n//4} = {N,n//2^2} QM structure, and it gives the Earth's outer core radius at the $(¾)^2 = 9/16$ of the Earth's radius, at the {-1,3//4} size with r ≈ 3.49E+6 meters (if using r_{Earth} = 6.38E+6 meters as the r_1, see SunQM-3s6); If more precisely, Earth can also belong to a {N,n//16} = {N,n/2^4} QM structure, and it gives Earth's inner core radius at the size of {-1,7//16}, Earth's outer core at the size of {-1,12//16}, and Earth's mantle at the size of {-1,15//16}, see SunQM-3s6's section I-i. Therefore, Earth's can be described by a {N,n//2^j} QM structure with the integer $j \ge 1$. The higher the j, the more precise the description. Here we used j = 8, or 2^8 = 256. We could have used 2^7, or 2^10, it does not really matter in this example). This means, we are using a {N,n//2^8} = {N,n//256} QM structure to describe the Earth's D(r). Let's move the r_1 to the size of {-1,1//256}, then, according to $r_n = r_1 * n\text{^}2$, the new $r_1 = r_{Earth} * (1 / 256)\text{^}2 = 6.38E+6 / 256\text{^}2 \approx 97$ meters (from the exact center of the Earth). So now, eq-17 becomes

$\sum_{n=1}^{n=256} \mathrm{D(r)} \; b'_n [r^2 |R(n,l)|^2] = \mathrm{D(r)}$ eq-19

In eq-19, we hope the $b'_n [r^2 |R(n,l)|^2]$ forms the unitary vector bases (i.e., the r_n at each n) of a Hilbert space (for each Δr of $r_n \le r < r_{n+1}$). For example, for the first five n(s), the unitary vector bases of each Δr space are: $1 \le r_{n=1} < 4$, $4 \le r_{n=2} < 9$, $9 \le r_{n=3} < 16$, $16 \le r_{n=4} < 25$. The function of $[r^2 |R(n,l)|^2]$ for the vector bases of n = 1 to n = 5 is shown in Figure 1a (with each *l* function showed separately), and also shown in Figure 4b (with all *l* functions summed for each n). We can see that for each vector base of the Δr space, its $b'_n [r^2 |R(n,l)|^2]$ function is always affected by its neighboring $b'_n [r^2 |R(n,l)|^2]$ functions. For example, for the (Hilbert space) vector base $r_{n=3}$ with Δr in $9 \le r_{n=3} < 16$, the corresponding function $[r^2 |R(n=3, l=0..2)|^2]$ only make the major (but not the 100%) contribution within $9 \le r_{n=3} < 16$. The neighboring functions at n =2, n =4, n =5, (i.e., $[r^2 |R(n=2, l=0..1)|^2]$, $[r^2 |R(n=4, l=0..3)|^2]$, $[r^2 |R(n=5, l=0..4)|^2]$) are all making small but

significant contribution (see Figure 4b). That is why I said that the $b'_n[r^2|R(n,l)|^2]$ functions (in eq-17, or in eq-10, or even in eq-2) are not the "good" vector base function, because they are always crossover with each other and thus have low convergency. Then, what is the "good" function for eq-17 (as the vector basis of the Hilbert space)? It should be something like

$$b'_n[r^2|R(n,l)|^2] = \begin{cases} 1, & r_n \le r < r_{n+1} \\ 0, & r < r_n \; and \; r \ge r_{n+1} \end{cases} \qquad \text{eq-20}$$

Interestingly, eq-20 is exactly what the rule of "all mass between r_n and r_{n+1} belongs to orbit n (see SunQM-3s2)" means. (Note: However, we know that this rule is only an approximation. Nature has already shown us that there are many (minor) violations of this rule: Jupiter has a {-1,n=1..4//5}o orbital n shell structure (if using $r_{Jupiter} = r_1$), and its outmost shell belongs to n=4 shell. However, the mass in the fast-moving zonal band (on the surface of Jupiter) belongs to the residue |5,4,m> QM state with n=5 (but not n=4, see Figure 4c, also see SunQM-3s3's Fig-4). The similar natural phenomenon has been seen in many times (see Appendix A for more examples). This means that under the gravitational force (where the Schrodinger equation using U ∝ 1/r, so it is suitable not only for G/RFg-force, but also for E/RFe-force), the rule of "all mass between r_n and r_{n+1} belongs to orbit n" is only an approximation, and the crossover $b'_n[r^2|R(n,l)|^2]$ functions are the real correct and accurate vector bases). Thus, if using eq-20, then the "unit vector base function" of eq-19 provided the information that the Earth's D(r) belongs to a {N,n//2^8} quantum structure.

Here is one guess: in eq-17, when r_1 is moved infinitely close to r = 0, its Hilbert space's vector bases (i.e., the eq-18) is infinitely close to eq-20.

Above is the discussion on how to use the eq-10 kind of equation (with a single N super shell) to reconstitute Earth's D(r) curve. Below is the discussion on how to use the eq-2 kind of equation (with many N super shells) to reconstitute Earth's D(r) curve. For Earth primary {N,n//2} QM structure (it means n ≡ 1), if we try to use Born probability radial function with n=1, and with many N super shells

$$\sum_{N\to-\infty}^{N\to\infty} a_N \left[\sum_{n=1}^{n=1} b_n {r_N}^2 |R(1,0)|^2\right] \qquad \text{eq-21}$$

to reconstitute the D(r) curve, the result is really poor. The reason is, eq-21 cannot fit to the cliff-drop in the Earth's D(r) curve, it can only produce the smooth declining and/or up-rising curve (data was not shown here). So, eq-21 may be fine to reconstitute either $|\vec{\mathbf{E}}|$ (∝ $1/r^2$) or U (∝ 1/r) curve, it is not fine for Earth's D(r) curve.

Although it doesn't work well with {N,n//2}, using eq-2 to fit to Earth's D(r) curve with {N,n//4}, or {N,n//8}, or {N,n//16}, it will be getting better and better. If fit with {N,n//2^8} = {N,n//256}

$$\sum_{N\to-\infty}^{N\to\infty} a_N \left[\sum_{n=1}^{n=255} b_n {r_N}^2 |R(n,l)|^2\right] \qquad \text{eq-22}$$

it should can fit well enough. However, it has no advantage to use eq-22 than to use eq-17, because the function of moving N → -∞ (to cover the r → 0 by using the multiple N super shells) in eq-22 is already fulfilled by moving the r_1 to very small in eq-17.

According to Figure 4a, using eq-2, the {N,n//4} QM structure of the Earth may can be expressed as

$$\sum_{N=-1}^{N=0} a_N \left[\sum_{n=1}^{n=3} b_n {r_N}^2 |R(n,l)|^2\right] = a_{N=-1}\left[\sum_{n=1}^{n=3} b_n {r_N}^2 |R(n,l)|^2\right] + a_{N=0}\left[b_{n=1} {r_{N=0}}^2 |R(1,0)|^2 + b_{n=2}\, {r_{N=0}}^2 |R(2,l)|^2 + b_{n=3} {r_{N=0}}^2 |R(3,l)|^2\right] \qquad \text{eq-23}$$

In eq-23, the last item $a_{N=0}[b_{n=3} {r_{N=0}}^2 |R(3,l)|^2]$ represents Earth's mantle (quantum) layer, the second last item $a_{N=0}[b_{n=2}\, {r_{N=0}}^2 |R(2,l)|^2]$ represents Earth's outer core (liquid iron) quantum layer, the third last item $a_{N=0}\left[b_{n=1} {r_{N=0}}^2 |R(1,0)|^2\right]$ represents the Earth's inner core (solid iron) quantum layer, the first item

$a_{N=-1}[\sum_{n=1}^{n=3} b_n {r_N}^2 |R(n,l)|^2]$ represents Earth's inner-inner core (that was predicted to have r ≈ 430 km, see SumQM-3s6's Table-6). Notice that eq-23 has the strongest quantum information of {N,n//4} QM in its unit vector base function.

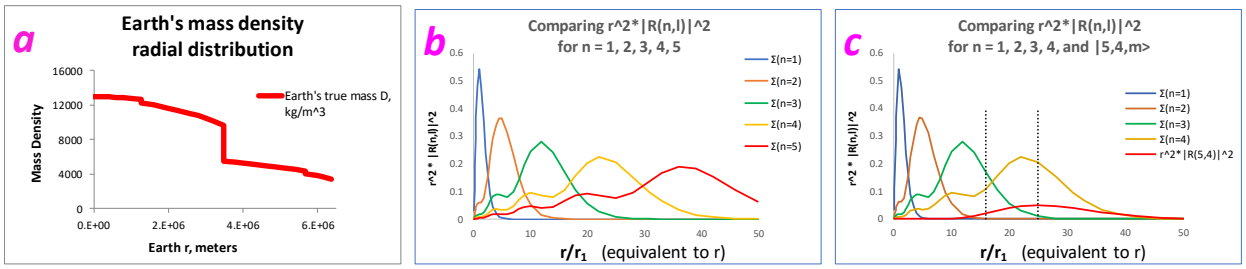

Figure 4a. Earth's true mass density curve D(r), obtained from wiki "Structure of the Earth", originally created by A. M. Dziewonski & D. L. Anderson (1981). (Also see SunQM-3s6's Fig-1b).

Figure 4b. Comparing radial Born probability density function $r^2|R(n,l)|^2$ for n = 1, 2, 3, 4, and 5 (with different l summed for each n).

Figure 4c. Comparing radial Born probability density function $r^2|R(n,l)|^2$ for |1,0,0>, |2,l,m>, |3,l,m>, |4,l,m> and |5,4,m> QM states. In the Δr range of $23 \le r/r_1 \le 25$ (i.e., the atmosphere near the surface of Jupiter), the |5,4,m> QM state (the red line curve intensity) makes the significant contribution on top of the |4,l,m> QM state (the orange line curve intensity).

IV. The physical meaning of eq-2 (in view of the wave mechanics)

First, let's review that how to use the wave mechanics to explain the Earth's orbital movement in the Solar system. In the solar system's {N,n//6} QM structure, Earth's r-1D position is fixed at {1,5//6} position. Under the wave mechanics, it means that Earth's r-1D matter wave is in the standing wave mode, with the out-going traveling wave (from r = 0 to r = ∞) interfered with the in-going traveling wave (from r = ∞ to r = 0), and produced the maximum wave intensity that standing at {1,5//6} position (see red line curve in Figure 4b for better understanding). So it is better to be described by the Born probability. Similarly, Earth's θ-1D position is fixed at θ = π/2. Under the wave mechanics, it means that Earth's θ-1D matter wave is in the standing wave mode, with the θ = 0 to θ = π traveling wave interfered with the θ = π to θ = 0 traveling wave, and produced the maximum wave intensity that standing at θ = π/2. So it is also better to be described by the Born probability. However, Earth's φ-1D position is not fixed at all, under the wave mechanics, it means that Earth's φ-1D matter wave is still in the traveling wave mode, so it should be described as the non-Born probability (NBP). (Also see the discussions in SunQM-4s1's section V). Now, let's forget the θ and φ dimensions, only consider r-1D dimension. For the eight known planets in the Solar system, in the r-1D, they are fixed at the {1,n=3..6//6} and {2,n=2..5//6} positions respectively. Under the wave mechanics, it means that there are 8 pairs of out-going and in-going traveling matter waves, and each pair of them produced a standing matter wave with the maximum intensity standing at the position in one of the {1,n=3..6//6} and {2,n=2..5//6} positions.

Figure 5a pretended to be a single point charge's static "electric field" (in 2D), with each (radiated) line represents a (radiated) radial wave function $r^2|R(n,l)|^2$ at either n = 1, or 2, or 3. The small ball at the far end of the radiated line represents the maximum Born probability position. (Note: Because each $r^2|R(n,l)|^2$ function starts from r = 0 and ends at r = ∞ (see Figure 4b for better understanding), for each radiated line, we should have drawn from r = 0 to r = ∞. However, it is impossible to draw a line to r = ∞, so I drew the line up to the max of the probability). Now, let's simplify the explanation: for each radial wave function, let's suppose that it only exerts the field effect at the maximum probability site (in r-1D). For example, the n=1 radial wave function is supposed to exert its field effect only within $1 \le r < 4$ (or, $r_n / r_1 = n^2$) range, the n=2 radial wave function is supposed to exert its field effect only within $4 \le r < 9$ range, and the n=3 radial wave function is supposed to exert its field effect only within (around) $9 \le r < 16$ range (see Figure 4b for better understanding. Note: this is similar as what eq-20 means). In other words, in eq-2, each $r^2|R(n,l)|^2$ function with different n only exert its field effect

within $r_n \le r < r_{n+1}$ range in r-1D space. (Note: In this simplified explanation, it is equivalent to the rule of "all mass between r_n and r_{n+1} belongs to orbit n (see SunQM-3s2)"). Then, in eq-2, the strength of the 2D "electric field" is determined by the number of the radial wave functions (i.e., the weight of the unit vector bases). For example, in Figure 5a, at r = 1 (or within $1 \le r < 4$), there are 16 of n=1 radial wave functions (vector bases), so the relative strength of this "electric field" (or "potential field") is 16; at r = 4 (or within $4 \le r < 9$), there are 8 of n=2 radial wave functions (vector bases), so the relative strength of this "electric field" (or "potential field") is 8; at r = 9 (or $9 \le r < 16$), there are 4 of n=3 radial wave functions (vector bases), so the relative strength of this "electric field" (or "potential field") is 4, and so on, so forth. (Note: The value of the $r^2|R(n,l)|^2$ function at each n quantum number is different, it is decreasing as the n number increasing (see Figure 4b). So, at the smaller r side of the r-1D space, the field strength is stronger not only because it has a greater number of radial wave functions, but also because each radial wave function (the vector base) has higher value).

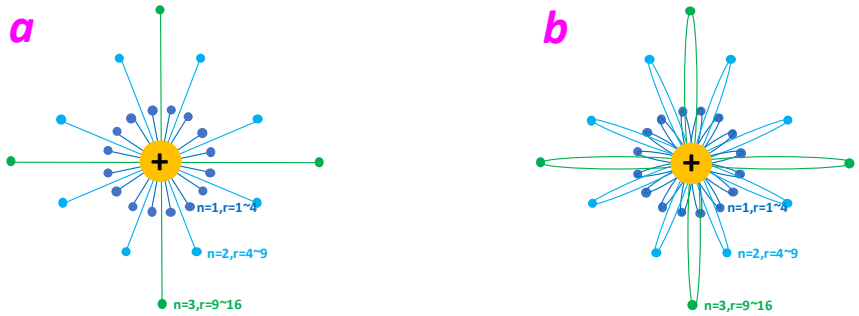

Figure 5a. Illustration of a (pretended) single point charge's 2D static "electric field", in view of the wave mechanics, with each (radiated) straight line represents a radial wave function $r^2|R(n,l)|^2$ at either n = 1, or 2, or 3, and the small ball represents the position where the maximum probability density located.
Figure 5b. Illustration of a (pretended) single point charge's 2D static "electric field", in view of the particle mechanics, with each small ball represents a particle (of electric force) that doing the ecliptic orbital movement around the (central) point charge, and the collection of the elliptical orbital trajectory forms the radial wave function $r^2|R(n,l)|^2$ probability density (at either n = 1, or 2, or 3).

With the example of Figure 5a, we now can use the wave mechanics to (intuitively) explain the physical meaning of eq-2 for the description of a point charge's static electric field $|\vec{\mathbf{E}}| \propto 1/r^2$. Let's use eq-5 (and the Table 4) as the example. Notice that the product of $a_N b_n$ in eq-5 is exactly the value of $1/r^2$ (in column 6 of Table 3). It means, in the r range of {-3,1//6}o orbital shell space (see Table 3 column 1~2), or in the r range of $1/36^3 \le r < 4/36^3$ (see Table 3 column 2~4), there are 2.18E+9 number of ${r_{N=-3}}^2|R(1,0)|^2$ Born probability radial functions (vector bases) to represent the (relative) strength of a point charge's static electric field $|\vec{\mathbf{E}}| \propto 1/r^2$; in the r range of {-3,2//6}o orbital shell space (see Table 3 column 1~2), or in the r range of $4/36^3 \le r < 9/36^3$ (see Table 3 column 2~4), there are 1.36E+8 number of ${r_{N=-3}}^2|R(2,l)|^2$ Born probability radial functions (vector bases) to represent the (relative) strength of the $|\vec{\mathbf{E}}| \propto 1/r^2$; in the r range of {-3,3//6}o orbital shell space, or in the r range of $9/36^3 \le r < 16/36^3$, there are 2.69E+7 number of ${r_{N=-3}}^2|R(3,l)|^2$ Born probability radial functions (vector bases) to represent the (relative) strength of the $|\vec{\mathbf{E}}| \propto 1/r^2$; … in the r range of {0,5//6}o orbital shell space, or in the r range of $25/36^0 \le r < 36/36^0$ (i.e., $25 \le r < 36$), there are $1/25^2 = 0.0016$ number of ${r_{N=0}}^2|R(5,l)|^2$ Born probability radial functions to represent the (relative) strength of the $|\vec{\mathbf{E}}| \propto 1/r^2$. In this way, we transformed a classical physics $|\vec{\mathbf{E}}| \propto 1/r^2$ field into a fully quantum (wave) mechanical represented form (as shown in eq-2, or exampled in eq-5).

V. The physical meaning of eq-2 (in view of the particle mechanics)

The same eq-2 can also be explained in view of the particle mechanics (see Figure 5b). (Note: Readers need to read SunQM-6s2's section-I before reading the current section. There, the H-atom's Born probability density 3D map of the electron was re-explained as the collection of the trajectory of a single electron's particle movement). For each $r^2|R(n,l)|^2$ function in eq-2 (that equivalent to each single line in Figure 5a), if we use one particle (named as the "**E-particle**") to represent its electric force, then the collection of the trajectory of this one E-particle's elliptical orbital movement will form a Born probability density (2D) map (as shown by any one of the single elliptical orbit in Figure 5b). Again, for each single $r^2|R(n,l)|^2$ function in eq-2 with a specific n, it can be approximated (or simplified) that it only exerts its force field effect within $r_n \le r < r_{n+1}$ range in r-1D space (at the aphelion site of its elliptical orbit, because the highest Born probability density). Again, in eq-2, the strength of the 2D static "electric field" is determined by the number of the radial wave functions that is now equivalent to the number of the E-particles. For example, in Figure 5b, within the range of $1 \le r < 4$, there are total 16 of n=1 radial wave functions (or E-particles), so the relative strength of this "electric field" (or "potential field") is 16; within the range of $4 \le r < 9$, there are total 8 of n=2 radial wave functions (or E-particles), so the relative strength of this "electric field" (or "potential field") is 8, and so on, so forth.

Therefore, the explanation of eq-5 (as an example of eq-2) is: in the r range of {-3,1//6}o orbital shell space, or in the r range of $1/36^3 \le r < 4/36^3$, there are total 2.18E+9 number of $r_{N=-3}{}^2|R(1,0)|^2$ Born probability radial functions (or E-particles) to represent the (relative) strength of the electric field $|\vec{\mathbf{E}}| \propto 1/r^2$; in the r range of {-3,2//6}o orbital shell space, or in the r range of $4/36^3 \le r < 9/36^3$, there are total 1.36E+8 number of $r_{N=-3}{}^2|R(2,l)|^2$ Born probability radial functions (or E-particles) to represent the (relative) strength of the electric field $|\vec{\mathbf{E}}| \propto 1/r^2$; and so on, so forth.

Before this description, there was always a major obstacle to use particle to explain the electric field (at least for me): because a single point charge's static electric field radiates from r = 0 to r = ∞ at the light speed, any trying of using particles (noticing that these particles must contain energy) to represent the static electric field will cause the particle to fly away (from the charge) to the infinity, and thus cause the charge to lose energy. (Note: This is similar as that in the old physics, the electromagnetic radiation of an orbiting electron in the planetary model of the atom will cause the electron to lose energy and then to spiral-in to crash to the nucleus [30]). If we used the Bohr-QM's circular orbit (like that the early QM did), it does not have any r-1D component, and thus cannot reflect the character of the electric field that propagating in r-1D at the light speed. Then, using the elliptical orbit, this obstacle has been removed, the (energy containing) E-particles are not completely moving away (from the point charge), they follow the elliptical orbit (notice that the 3D elliptical orbital motion is equivalent to an oscillation motion in r-1D), so that the radiation of them do have the component in r-1D space, but do not lose the energy of a single point charge's static electric field. Remember that all these elliptical orbits follow the Born probability density map, so it become a perfect description.

VI. In the view of wave mechanics, a point-centered field (that can be described with eq-2) should can also be described by the 3D spherical wave packet

In {N,n} QM field theory, everything (i.e., both the point-centered mass field and the point-centered force field) can be described in the form of 3D spherical wave packet. SunQM-6s2's Fig-6a (that was copied here as the Figure 6b) showed that how a 1D wave packet looks like. Before, we don't really know the detailed structure of a 3D spherical wave packet (except it has onion-like multiple shells). Now, with the help of eq-2, we try to look into the detail. If we degenerate a rθφ-3D spherical wave packet (with many n shells and N super shells) into r-1D, each one n shell of the 3D spherical wave packet should look like Figure 6b. For the 2D pseudo "electric field" in Figure 5a (now we can think it as the 3D pseudo "electric field"), once we degenerate it into r-1D (not with $0 < r < \infty$, but with $-\infty < r < \infty$), then each one n shell should have the ±r 1D wave function with two peaks as shown in Figure 6a. (Notice that Figure 6a was constructed with Figure 4b with a mirroring operation along y-axis). By comparing Figure 6a to Figure 6b, we can easily understand that the two blue line curve peaks (of the Born probability density at n=1) in Figure 6a represent the two edge of an n=1 QM state rθφ-3D spherical wave packet (of the Born probability density). (Note: it looks like a spherical shell with a hollow center). Then, the two dark-orange line curve peaks (of the Born probability density at n=2) in Figure 6a represent the two edge of a n=2 QM state (a shell-like) 3D

spherical wave packet (of the Born probability density), and then, one-by-one, the two green peaks at n=3, the two light-orange peaks at n=4, and the two red peaks at n=5 in Figure 6a, each represent the two edge of an n=3 (shell-like), n=4 (shell-like), and n=5 (shell-like) rθφ-3D spherical wave packet (of the Born probability density) respectively. Then, after combining all of them, the whole rθφ-3D spherical wave packet (of the Born probability density) with a structure of n = 1, 2, 3, 4, 5 shells (within one N super shell of a {N,n//6} QM structure) was depictured in Figure 6c. (Note: in Figure 6c, the n = 1 core of the 3D spherical wave packet is not shown, because it belongs to the ΔN = -1 super shell in a {N,n//6} QM structure).

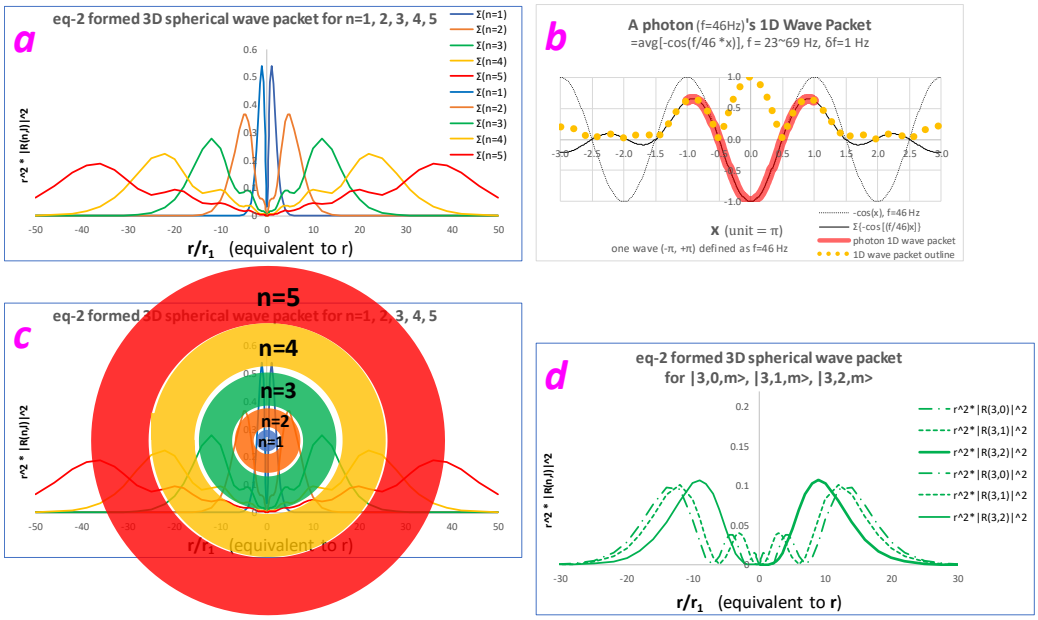

Figure 6a. To illustrate the eq-2 formed 3D spherical wave packet (for n = 1, 2, 3, 4, 5) that is viewed in ±r 1D.
Figure 6b. Copied from SunQM-6s2's Fig-6a, to show a 1D wave packet (with its "main" wavelength is shown in the red thick line curve).
Figure 6c. To illustrate the eq-2 formed 3D spherical wave packet (for n = 1, 2, 3, 4, 5) that is viewed in 2D.
Figure 6d. To illustrate the eq-2 formed 3D spherical wave packet (for n = 3 shell only) that can be further divided into 3 sub-shells of 3D spherical wave packet (viewed in ±r 1D).

Note: As shown in Figure 6c, the thickness of each n shell (of 3D spherical wave packet) is very thick, and it covers (at least) from r_n to r_{n+1}, so that there is no gap left in between of these shells. We can see the same thing in Figure 6a, the all the probability density peaks are very broad so that no gap is left in between. However, it is inaccurate to say that "all probability between r_n to r_{n+1} belongs to n QM state" (note: this saying is equivalent to eq-20), instead, it is correct to say that "**for the general point-centered field's 3D spherical wave packet, the main probability between r_n to r_{n+1} belongs to n QM state**" (note: this saying is equivalent to eq-2). Similarly, it is correct to say that "for a point-centered mass field's 3D spherical wave packet, the mass between r_n to r_{n+1} mainly belongs to orbit n" (note: this saying is equivalent to eq-2). Although the rule of "all mass between r_n to r_{n+1} belongs to n orbit" is still fine to use in many cases if the low accuracy is enough (because it does greatly simplify the explanation).

According to the result of SunQM-6s2's Fig-6a, in the wave mechanics, each 3D spherical wave packet (of the Born probability density), or each shell, has the "main" or the "effective" wavelength λ_n (approximately) equals to the diameter of this spherical shell, or $\lambda_n \approx 2r_n$. Therefore, from Figure 6a, we can easily read out the (approximate) "main" wavelength of each 3D spherical wave packet, such as for |3,*l*,m> , |4,*l*,m> , |5,*l*,m> QM states, $\lambda_{n=3} \approx 2r_{n=3} \approx 24$, $\lambda_{n=4} \approx 2r_{n=4} \approx 46$, and $\lambda_{n=5} \approx 2r_{n=5} \approx 74$, respectively. Because the matter wave's frequency $f_n \propto 1/\lambda_n$, and the matter wave's energy $E_n \propto f_n$, so the inner

shell of the 3D spherical wave packet has the lower n quantum number, the shorter λ_n , the higher field f_n, and the higher field energy, and vice versa.

The 3D spherical wave packet description is not only valid for each n shell, but also valid for each *l* sub-shell (see Figure 6d), and even valid for each N super shell (figure not shown). For example, in Figure 6d, it showed that in the n = 3 shell of the 3D spherical wave packet, it can still be further divided into three sub-shells. They are (from inner to outer): |3,2,m> sub-shell, |3,1,m> sub-shell, and |3,0,m> sub-shell. Again, for each sun-shell of the 3D spherical wave packet, we can easily read out its (approximate) "main" wavelength. For example, for the |3,2,2> , |4,3,3> , |5,4,4> QM states correlated 3D spherical wave packet sub-shell, it has $\lambda_{n=3} \approx 2*9 = 18$, $\lambda_{n=4} \approx 2*16 = 32$, and $\lambda_{n=5} \approx 2*25 = 50$, respectively. (Note: For the general |n,*l*,m>, its r_n of the maximum probability is greater than $r_n = r_1 n^2$. Only for nLL, its r_n of the maximum probability is exactly same as $r_n = r_1 n^2$).

Then, what is the difference between the eq-2 reconstitution and the 3D spherical wave packet representation (since both of them are based on {N,n} QM structure)? By comparing Figure 5a and Figure 6d, they have practically the same morphology for all n shells, but with different weighting number for each n shell. Then, learned from the explanation of Figure 5a, we can treat each n shell of the 3D spherical wave packet in Figure 6d as a "unit vector base" for a high-dimensional Hilbert space (that covers from $r \rightarrow 0$ to $r = \infty$). By using different set of weighting numbers, the 3D spherical wave packet can be used to describe either the $\left|\vec{\mathbf{E}}\right| \propto 1/r^2$ field, or the $U \propto 1/r$ field, or the Sun core's $D \approx 1.26 \times 10^{23} \frac{1}{r^{2.33}}$ (kg/m^3) mass field, etc., (just like what the eq-2 did). For example, according to Table 3, by using the weighting number of 2.18E+9 for the {-3,1//6}o orbital n shell, and 1.36E+8 for the {-3,2//6}o orbital n shell, ... , this (weighted) 3D spherical wave packet is perfect to describe the $\left|\vec{\mathbf{E}}\right| \propto 1/r^2$ field. Alternatively, by using the weighting number of 46656 for the {-3,1//6}o orbital n shell, and 11664 for the {-3,2//6}o orbital n shell, ... , this (weighted) 3D spherical wave packet is perfect to describe the $U \propto 1/r$ field. In this way, these two description methods, the eq-2 reconstitution and the (weighted) 3D spherical wave packet representation, are completely equivalent and switchable.

Notice that this eq-2 described (or eq-2 weighted) 3D spherical wave packet is valid not only for the point charge's static electric field, but also for the electromagnetic field (i.e., the photon particle), the point-centered G/RFg-force field, the point-centered mass field, etc. Here are some examples:

1) A single proton's positive charge generated static electric field can be described by this (weighted) 3D spherical wave packet;
2) According to the text book [31], a single charge (named as Q)'s electric field $\vec{\mathbf{E}}$ is defined as this charge Q's electric force field $\vec{\mathbf{F}}$ divided by the magnitude of a tiny test charge q: $\vec{\mathbf{E}} = \vec{\mathbf{F}}/q$. So, it is obvious that for a tiny test charge q, a single charge Q's 3D pattern of the force field $\vec{\mathbf{F}}$ should be (almost exactly) the same as that of the 3D pattern of the electric field $\vec{\mathbf{E}}$, and thus can be described by this (weighted) 3D spherical wave packet;
3) In an H-atom, the collection of the motion trajectory of the electron that orbiting around the proton (and that formed Born probability density map) can be described by this (weighted) 3D spherical wave packet; This also means, in an H-atom, a pair of (the heavy) proton and (the light) electron generated E/RFe-force field in the {N=-3..0,n=1..5//6}o orbital shell space (centered on the proton, using Bohr radius $a_0 = r_1$) may can be described by this (weighted) 3D spherical wave packet;
4) In an H-atom, an orbital moving electron itself can be described by this (weighted) 3D spherical wave packet (see SunQM-6s2's section II-b); Similarly, a single proton itself can be described by this (weighted) 3D spherical wave packet;
5) In an H-atom, an orbital moving electron de-excited from n=3 to n=2 orbit, and spun-off its outmost shell of the 3D spherical wave packet (of the E/RFe-force field) as a new born photon, and this photon's E/RFe-force field (or the electromagnetic field) can also be described by the (weighted) 3D spherical wave packet (see SunQM-6s2's Fig-7j, Fig-7k, also see SunQM-6s5's Fig-6);
6) In the Solar system, our Sun generated G/RFg-force field in the {N=0..4,n=1..5//6}o orbital shell space (using Sun core's radius as r_1) can be described by this (weighted) 3D spherical wave packet;
7) Not only the G/RFg-force field, but also the mass field generated by our Sun in the {N=0..4,n=1..5//6}o orbital shell space (using Sun core's radius as r_1) can also be described by this (weighted) 3D spherical wave packet;
8) An ancient planet Triton generated G/RFg-force field can be described by this (weighted) 3D spherical wave packet;

9) When the ancient planet Triton (at {2,6//6} orbit) was captured by the planet Neptune (at {2,5//6} orbit), the de-exciting from n=6 to n=5 orbit made Triton to spin-off its outmost shell of the 3D spherical wave packet (of the G/RFg-force field) as a new born G-photon, and this G-photon's G/RFg-force field can also be described by the (weighted) 3D spherical wave packet (see SunQM-6s2's Fig-1).

VII. More discussions

1) Using eq-2 to reconstitute any point-centered field (like $|\vec{\mathbf{E}}| \propto 1/r^2$ or $U \propto 1/r$) is an intrinsic property (or the natural attribute) of {N,n//q} QM field theory, and it can be used with q number from q = 2, 3, 4, 5, 6, 7, etc. For example: a {N,n//6} QM may be appropriate for the reconstitution of a proton's electric field for an H-atom; a {N,n//7} QM may be appropriate for the reconstitution of the nucleus's electric field for a Xe atom (Z = 54).
2) From the mathematic point view of the Hilbert space, the Born probability formed "unit vector base functions" in the eq-2 has a "low quality", because each vector base contains some (impurity) contamination from the neighboring vector bases (if each N super shell contains only a few n shells). However, from the point view of the {N,n} QM field theory, it is a great success, because it has provided a generalized way so that all point-center fields can be reconstituted by using Schrodinger equation/solution.
3) In SunQM-6s1's Fig-3, when using the 3D wave packet to describe a photon's propagation, its core propagates with the light speed c, its wave-front propagates with 2c, its wave-tail propagates with 0c. This means, when we set the coordinate at the photon's core, this photon's electromagnetic field radiates from the point center of the photon to all 4π directions in the light speed c, and it is just like a single point charge's static electric field radiates to all 4π directions in the light speed c. Thus, everything make sense. Therefore, it added one more positive point to the {N,n} QM field theory.
4) The 3D wave packet description perfectly explained the wave-particle duality for all fields (including the mass field, force field, etc.): while the core of the 3D wave packet reflects the particle character of the field, the outer shells of the 3D wave packet reflect the wave character of the field (also see SunQM-6s1's section III-d).
5) All above discussions are based on the H-atom's Schrodinger equation/solution (with the attractive potential function of $U \propto -1/r$). Can we put other "potential" function (e.g., 1/r^2, or something like eq-20, or the repulsive potential) into the Schrodinger equation (and still keep the energy conservation) to obtain the new kind of radial wave function? I tried the repulsive potential one time, but failed (due to my math is not high enough, as a citizen scientist).
6) So far, the 3D spherical wave packet constructed in Figure 6 is mostly by visual. It still needs mathematician to prove it in a mathematical way.

Conclusion

Finally, this paper figured out how to use the Schrodinger equation/solution (in the form of Born probability) to reconstitute the electric field equation $|\vec{\mathbf{E}}| = \frac{q}{4\pi\epsilon_0}\frac{1}{r^2}$ and the potential equation $|U| = \frac{q}{4\pi\epsilon_0}\frac{1}{r}$. And, all point-centered field can be represented in the form of 3D spherical wave packet. And, there two descriptions are equivalent.

Acknowledgements:

Many thanks to: all the (related) experimental scientists who produced the (related) experimental data, all the (related) theoretical scientists who generated all kinds of theories (that become the foundation of {N,n//q} QM theory), the (related) text book authors who wrote down all results into a systematic knowledge, the (related) popular science writers who

simplified the complicated modern physics results into a easily understandable text, the (related) Wikipedia writers who presented the knowledge in a easily accessible way, the (related) online (video/animated) course writers/programmers who presented the abstract knowledge in an intuitive and visually understandable way. Also thanks to NASA and ESA for opening some basic scientific data to the public, so that citizen scientists (like me) can use it. Also thanks to the online preprinting serve vixra.org to let me post out my original SunQM series research articles.

Special thanks to: Fudan university, theoretical physics (class of 1978, and all teachers), it had made my quantum mechanics study (at the undergraduate level) become possible. Also thanks to Tsung-Dao Lee and Chen-Ning Yang, they made me to dream to be a physicist when I was eighteen. Also thanks to Shoucheng Zhang (张首晟, Physics Prof. in Stanford Univ., my classmate at Fudan Univ. in 1978) who had helped me to introduce the {N,n} QM theory to the scientific community.

Also thanks to a group of citizen scientists for the interesting, encouraging, inspiring, and useful (online) discussions: "职老" (https://bbs.creaders.net/rainbow/bbsviewer.php?trd_id=1079728), "MingChen99" (https://bbs.creaders.net/tea/bbsviewer.php?trd_id=1384562), "zhf" (https://bbs.creaders.net/tea/bbsviewer.php?trd_id=1319754), Yingtao Yang (https://bbs.creaders.net/education/bbsviewer.php?trd_id=1135143), "tda" (https://bbs.creaders.net/education/bbsviewer.php?trd_id=1157045), etc.

Also thanks to: Takahisa Okino (Correlation between Diffusion Equation and Schrödinger Equation. Journal of Modern Physics, 2013, 4, 612-615), Phil Scherrer (Prof. in Stanford University, who explained WSO data to me (in email, see SunQM-3s9)), Jing Chen (https://www.researchgate.net/publication/332351262_A_generalization_of_quantum_theory), etc. Note: if I missed anyone in the current acknowledgements, I will try to add them in the SunQM-9s1's acknowledgements.

Reference:

[1] Yi Cao, SunQM-1: Quantum mechanics of the Solar system in a {N,n//6} QM structure. http://vixra.org/pdf/1805.0102v2.pdf （original submitted on 2018-05-03）

[2] Yi Cao, SunQM-1s1: The dynamics of the quantum collapse (and quantum expansion) of Solar QM {N,n} structure. http://vixra.org/pdf/1805.0117v1.pdf （submitted on 2018-05-04）

[3] Yi Cao, SunQM-1s2: Comparing to other star-planet systems, our Solar system has a nearly perfect {N,n//6} QM structure. http://vixra.org/pdf/1805.0118v1.pdf （submitted on 2018-05-04）

[4] Yi Cao, SunQM-1s3: Applying {N,n} QM structure analysis to planets using exterior and interior {N,n} QM. http://vixra.org/pdf/1805.0123v1.pdf （submitted on 2018-05-06）

[5] Yi Cao, SunQM-2: Expanding QM from micro-world to macro-world: general Planck constant, H-C unit, H-quasi-constant, and the meaning of QM. http://vixra.org/pdf/1805.0141v1.pdf （submitted on 2018-05-07）

[6] Yi Cao, SunQM-3: Solving Schrodinger equation for Solar quantum mechanics {N,n} structure. http://vixra.org/pdf/1805.0160v1.pdf （submitted on 2018-05-06）

[7] Yi Cao, SunQM-3s1: Using 1st order spin-perturbation to solve Schrodinger equation for nLL effect and pre-Sun ball's disk-lyzation. http://vixra.org/pdf/1805.0078v1.pdf （submitted on 2018-05-02）

[8] Yi Cao, SunQM-3s2: Using {N,n} QM model to calculate out the snapshot pictures of a gradually disk-lyzing pre-Sun ball. http://vixra.org/pdf/1804.0491v1.pdf （submitted on 2018-04-30）

[9] Yi Cao, SunQM-3s3: Using QM calculation to explain the atmosphere band pattern on Jupiter (and Earth, Saturn, Sun)'s surface. http://vixra.org/pdf/1805.0040v1.pdf （submitted on 2018-05-01）

[10] Yi Cao, SunQM-3s6: Predict mass density r-distribution for Earth and other rocky planets based on {N,n} QM probability distribution. http://vixra.org/pdf/1808.0639v1.pdf (submitted on 2018-08-29)

[11] Yi Cao, SunQM-3s7: Predict mass density r-distribution for gas/ice planets, and the superposition of {N,n//q} or |qnlm> QM states for planet/star. http://vixra.org/pdf/1812.0302v2.pdf (replaced on 2019-03-08)

[12] Yi Cao, SunQM-3s8: Using {N,n} QM to study Sun's internal structure, convective zone formation, planetary differentiation and temperature r-distribution. http://vixra.org/pdf/1808.0637v1.pdf (submitted on 2018-08-29)

[13] Yi Cao, SunQM-3s9: Using {N,n} QM to explain the sunspot drift, the continental drift, and Sun's and Earth's magnetic dynamo. http://vixra.org/pdf/1812.0318v2.pdf (replaced on 2019-01-10)

[14] Yi Cao, SunQM-3s4: Using {N,n} QM structure and multiplier n' to analyze Saturn's (and other planets') ring structure. http://vixra.org/pdf/1903.0211v1.pdf (submitted on 2019-03-11)

[15] Yi Cao, SunQM-3s10: Using {N,n} QM's Eigen n to constitute Asteroid/Kuiper belts, and Solar {N=1..4,n} region's mass density r-distribution and evolution. http://vixra.org/pdf/1909.0267v1.pdf (submitted on 2019-09-12)

[16] Yi Cao, SunQM-3s11: Using {N,n} QM's probability density 3D map to build a complete Solar system with time-dependent orbital movement. https://vixra.org/pdf/1912.0212v1.pdf (original submitted on 2019-12-11)
[17] Yi Cao, SunQM-4: Using full-QM deduction and {N,n} QM's non-Born probability density 3D map to build a complete Solar system with orbital movement. https://vixra.org/pdf/2003.0556v2.pdf (replaced on 2021-02-03)
[18] Yi Cao, SunQM-4s1: Is Born probability merely a special case of (the more generalized) non-Born probability (NBP)? https://vixra.org/pdf/2005.0093v1.pdf (submitted on 2020-05-07)
[19] Yi Cao, SunQM-4s2: Using {N,n} QM and non-Born probability to analyze Earth atmosphere's global pattern and the local weather. https://vixra.org/pdf/2007.0007v1.pdf (submitted on 2020-07-01)
[20] Yi Cao, SunQM-5: Using the Interior {N,n//6} QM to Describe an Atom's Nucleus-Electron System, and to Scan from Sub-quark to Universe (Drafted in April 2018). https://vixra.org/pdf/2107.0048v1.pdf (submitted on 2021-07-06)
[21] Yi Cao, SunQM-5s1: White Dwarf, Neutron Star, and Black Hole Explained by Using {N,n//6} QM (Drafted in Apr. 2018). https://vixra.org/pdf/2107.0084v1.pdf (submitted on 2021-07-13)
[22] Yi Cao, SunQM-5s2: Using {N,n//6} QM to Explore Elementary Particles and the Possible Sub-quark Particles. https://vixra.org/pdf/2107.0104v1.pdf (submitted on 2021-07-18)
[23] Yi Cao, SunQM-6: Magnetic force is the rotation-diffusion (RF) force of the electric force, Weak force is the RF-force of the Strong force, Dark Matter may be the RF-force of the gravity force, according to a newly designed {N,n} QM field theory. https://vixra.org/pdf/2010.0167v1.pdf (replaced on 2020-12-17, submitted on 2020-10-21)
[24] Yi Cao, SunQM-6s1: Using Bohr atom, {N,n} QM field theory, and non-Born probability to describe a photon's emission and propagation. https://vixra.org/pdf/2102.0060v1.pdf (submitted on 2021-02-11)
[25] Yi Cao, SunQM-7: Using {N,n} QM, Non-Born-Probability (NBP), and Simultaneous-Multi-Eigen-Description (SMED) to describe our universe. https://vixra.org/pdf/2111.0086v1.pdf (submitted on 2021-11-17)
[26] Yi Cao, SunQM-6s2: A Unified Description Of 1D-Wave, 1D-Wave Packet, 3D-Wave, 3D-Wave Packet, and |nlm> Elliptical Orbit For A Photon's Emission and Propagation Using {N,n} QM. https://vixra.org/pdf/2208.0039v1.pdf (submitted on 2022-08-08)
[27] Yi Cao, SunQM-6s3: Using {N,n} QM and "|nL0> Elliptical/Parabolic/Hyperbolic Orbital Transition Model" to Describe All General "Decay" Processes (Including the Emission of a Photon, a G-photon, or An Alpha-particle). (submitted on 2022-08-31, but has not been able to get posted out, I don't know the reason)
[28] **梁昆淼, 数学物理方法**, (Kun-miao Liang, Methods of Mathematical Physics) 1978, 2nd ed.
[29] Note: I forgot from which course or from which book that I had learned this (over 40 years ago).
[30] Stephen T. Thornton & Andrew Rex, Modern Physics for Scientists and Engineers, 3rd ed. 2006. p141, Fig-4.14.
[31] Douglas C. Giancoli, Physics for Scientists & Engineers with Modern Physics, 4th ed. 2009, p568, eq-21-3.

Note: A series of SunQM papers that I am working on:
SunQM-6s5: Using {N,n} QM Field Theory to Describe A Propagating Photon with … (drafted in Jan. 2023).
SunQM-6s6: Using {N,n} QM Field Theory to Study the Atomic Electron … (drafted in Apr. 2023).
SunQM-6s7: {N,n} QM Field Theory Development On the E/RFe-force … (drafted in Apr. 2023).
SunQM-6s8: {N,n} QM Field Theory Development On the G/RFg-force … (drafted in Apr. 2023).
SunQM-6s9: {N,n} QM Field Theory Development On the S/RFs-force … (drafted in May. 2023).
SunQM-6s10: Schrodinger equation and {N,n} QM ... (drafted in January 2020).
SunQM-4s4: More explanations on non-Born probability (NBP)'s positive precession in {N,n}QM.
SunQM-7s1: Relativity and non-linear {N,n} QM
SunQM-9s1: Addendums, Updates and Q/A for SunQM series papers.

Note: Major QM books, data sources, software I used for SunQM series papers study:
Douglas C. Giancoli, Physics for Scientists & Engineers with Modern Physics, 4th ed. 2009.
David J. Griffiths, Introduction to Quantum Mechanics, 2nd ed., 2015.
Stephen T. Thornton & Andrew Rex, Modern Physics for Scientists and Engineers, 3rd ed. 2006.
John S. Townsend, A Modern Approach to Quantum Mechanics, 2nd ed., 2012.
James Binney & David Skinner, The Physics of Quantum Mechanics, 1st ed. 2014.
Wikipedia at: https://en.wikipedia.org/wiki/
(Free) online math calculation software: WolframAlpha (https://www.wolframalpha.com/)
(Free) online spherical 3D plot software: MathStudio (http://mathstud.io/)
(Free) offline math calculation software: R
Microsoft Excel, Power Point, Word.
Public TV's space science related programs: PBS-NOVA, BBC-documentary, National Geographic-documentary, etc.
Journal: Scientific American.

Note: I am still looking for endorsers to post all my SunQM papers (including the future papers) to arXiv.org. Thank you in advance!

Note: With my 28 of SunQM papers that have been posted out so far, I believe that the framework of the {N,n} QM has been fully established. It is clear now that the {N,n} QM description is not only suitable for the mass field, but also suitable for the force field (or potential field, or energy field, etc.). Thus, my (10 years of close-door) research phase on the {N,n} QM will be ended in about one year (most likely in the summer of 2024). After that, I will re-write the SunQM papers (~ 35 of them) in the form of a text book. Both the section III and the Appendix A of this paper will be re-written as the questions/excises at the end of one chapter of the text book.

Appendix A. A list of examples that (minorly) violate the rule of "all mass between r_n and r_{n+1} belongs to orbit n".

1) If we treat the Earth's as the pure {N,n//2} QM structure, e.g., treat the Earth's inner core as the {-1,1//2} sized QM structure (with $r_{Earth} = r_1$), and treat the Earth's mantle layer plus the outer core layer as the {-1,1//2}o orbital shell QM structure (note: this means that the mass in both the mantle layer and the outer core layer is in the |1,0,0> QM state), and treat the Earth's atmosphere (the troposphere only) as a compressed {0,1//2}o orbital shell QM structure (note: this means that the mass in troposphere is also in the |1,0,0> QM state), then the polar jet stream may can be treated as the residue n=2 QM state with the |2,1,1> QM mode that are embedded in the background layer of |1,0,0> QM state (i.e., the troposphere). (Note: {N,n//2} should be the strong {N,n//q} QM mode for the Earth's atmosphere). Alternatively, as shown in SunQM-4s2's Fig-3, we can treat Earth as a {N,n//3} QM structure, with the Earth core as the {-1,1//2} = {-1,1//3} sized QM structure (with $r_{Earth} = r_1$), and treat the Earth's mantle plus layer the outer core layer as the {-1,1//2}o = {-1,1//3}o orbital shell QM structure (note: this means that the mass in both mantle layer and the outer core layer is in the |1,0,0> QM state), and then treat the Earth's atmosphere (the troposphere only) as a compressed {-1,2//3}o orbital shell QM structure (note: this means that the mass in troposphere is in the |2,*l*,m> QM state), then the polar jet stream may can be treated as the residue |3,2,0> QM state, and the subtropical jet stream may can be treated as the residue |3,2,1> QM state, and both are embedded in the background layer of |2,0,0> QM state (i.e., the tropopause at the out-edge of the troposphere, see SunQM-4s2's Fig-3). Notice that both polar jet residue |3,2,0> and subtropical jet residue |3,2,1> are moving eastward faster than that of the background mass that is in |2,0,0> QM mode. (Note: {N,n//3} should be the weak {N,n//q} QM mode for the Earth's atmosphere). Because the polar jet stream shows up in (or it is the superposition QM state of) both Earth atmosphere's strong {N,n//2} QM mode and the weak {N,n//3} QM mode, while the subtropical jet stream shows up only in Earth atmosphere's weak {N,n//3} QM mode, this caused the polar jet stream to behave as a strong jet stream, and the subtropical jet stream to behave as a weak jet stream.

2) As shown in SunQM-4s2, Jupiter has a {-1,n=1..4//5}o orbital n shell structure (if using $r_{Jupiter} = r_1$), and its outmost n shell belongs to n=4 shell with |4,*l*,m> QM state, and the outmost *l* sub-shell belongs to |4,0,0> QM mode. However, the mass in the fast-moving zonal bands (on the surface of Jupiter) belong to the residue |5,4,m> QM state (i.e., |5,4,4>, |5,4,±3>, |5,4,±2>, |5,4,±1>, seven of them) with n=5 (but not n=4, see SunQM-3s3's Fig-4). Notice that these seven zonal bands are moving eastward faster than that of the background mass (i.e., the belt bands) that is in |4,0,0> QM mode. (Note: In comparison with the Earth atmosphere's polar jet stream vs. the subtropical jet stream, all seven zonal bands on the Jupiter are similar as Earth's polar jet stream. The Earth's subtropical jet equivalent stream should be in the Jupiter's belt band region and they are too weak to show up, see SunQM-3s3's Fig-4).

3) In the pre-Sun ball that at the size of {3,1//6} = {2,6//6}, although the majority mass in the outmost n shell of {2,5//6}o orbital shell was at n=5 QM state (and after collapsing, the leftover mass accreted to be Neptune), there was minority mass in the outmost n shell of {2,5//6}o orbital shell was at the residue n=6 QM state, or the residue |6,5,m> QM state (and after collapsing, the leftover mass formed Pluto and the Kuiper belt, see SunQM-7's Appendix B).

4) Similarly, in the pre-Sun ball that at the size of {2,1//6} = {1,6//6}, although the majority mass in the outmost n shell of {1,5//6}o orbital shell was at n=5 QM state (and after collapsing, the leftover mass accreted to be Earth), there was minority mass in the outmost n shell of {1,5//6}o orbital shell was at the residue n=6 QM state, or the residue |6,5,m> QM state (and after collapsing, the leftover mass formed Mars and the Asteroid Belt at the position of {1,6//6}o orbital n shell space. Note: then the Asteroid Belt moved to the current position of {1,8//6}o orbital n shell space, see SunQM-7's Appendix B).

5) Although the Sun core was initially determined to have 20% ~ 25% of the Sun radius (see wiki "Sun"), according to the Solar {N,n//6} QM structure, it should have ~ 25% of the Sun radius (see SunQM-1). Using Sun core's radius as r_1, the Sun mass at the outside of the Sun core occupies the {0,1//6}o orbital shell space with n=1, or at the |1,0,0> QM state. According to the standard {N,n} QM structure, part of the mass at the equator of the Sun's surface must be in the residue |2,1,1> QM state (that has the eastward faster movement than the background |1,0,0> QM state). As shown in SunQM-3s9's Fig-1, on the Sun surface, the evolution of the sunspot drifting is driven by this residue |2,1,1> QM state that further evolved to be the residue |3,2,2>, then to |4,3,3>, |5,4,4>, … |72,71,71> residue QM state, one by one, or evolved to high n quantum number but still in the (residue) nLL QM mode.

6) Similarly, if using $r_{Earth} = r_1$, Earth's mantle shell can be described as {-1,3//4}o orbital shell with n=3, or |3,*l*,m> QM mode, and with the outmost *l* sub-shell at the |3,0,0> QM mode. According to the standard {N,n} QM structure, part of the mass at the equator of Earth mantle shell's surface must be in the residue n=4 QM state with the residue |4,3,3> QM mode (that has the eastward faster movement than the background |3,0,0> QM state). This fast-moving residue |4,3,3> QM mode further evolved to be higher n quantum numbered residue nLL QM state, like the residue |5,4,4>, |6,5,5>, etc., and thus causes the Earth's continents (on top of the Earth's mantle shell) to drift (also see SunQM-3s9).

7) From the above examples, we can see that in the standard {N,n//q} QM structure, for a (point-centered) mass ball with the outmost shell in n QM state, at the surface equator of this mass ball, there is always some residue mass that is in the nLL mode but at a higher n QM state (usually in the n+1 QM state). We named this as the "**residue**" nLL mode. This residue nLL mode (that is in the |n+1,n,n> QM state) is embedded (or inlaid) on the surface of the (background) n shell, and it has the faster moving speed than that of the background mass (that is in the n QM state). Of course, this phenomenon only happens in a self-spinning mass ball. Although (so far) this phenomenon is observed only for a self-spinning mass ball (i.e., a point-centered self-spinning mass field), I believe that it should happen for any point-centered self-spinning field, including the point-centered self-spinning force field (see in SunQM-6s5 and SunQM-6s7).

8) One interesting question: we know that Earth was accreted from the < 1% leftover mass in the {1,5//6}o orbit shell space (after the {2,1//6} sized pre-Sun ball collapsed to be the {1,1//6} sized pre-Sun ball), but now, should we treat the Earth as the |5,4,4> QM state in the {1,5//6}o orbital shell, or, as the residue |5,4,4> QM mode that embedded on the surface of the {1,4//6}o orbital shell?